Olfactory Transduction and Taste Processing in Drosophila

Dissertation Advisor: Rachel Wilson Yi Zhou

Olfactory Transduction and Taste Processing in *Drosophila*

Abstract

We completed two separate studies examining chemosensation in *Drosophila*. The first study investigated taste processing. It was our aim in this study to identify and characterize higher-order gustatory neurons. Our strategy for tackling this problem involved complementary functional and anatomical approaches. First, we used calcium imaging to screen for cells responding to stimulation of gustatory receptor neurons. Second, we used photo-activatable GFP to localize the cell bodies of neurons innervating the gustatory neuropil. Third, based on the information we gained from these imaging experiments, we were able to identify some promising Gal4 lines that labeled candidate gustatory neurons. Fourth and finally, we made whole-cell patch clamp recordings from these candidate gustatory neurons while stimulating the proboscis with tastants. Unfortunately, none of these candidates turned out to be gustatory neurons. However, this study illustrates a flexible and powerful general approach to identifying and characterizing sensory neurons in the *Drosophila* brain.

The second study investigated olfactory transduction. Specifically, we examined the effect of air speed on olfactory receptor neuron responses (ORNs) in *Drosophila*. We constructed an odor delivery device that allowed us to independently vary concentration and air speed, and we used a fast photoionization detector to precisely measure the actual odor concentration at the antenna while simultaneously recording spikes from ORNs *in vivo*. Our results demonstrate that *Drosophila* ORN odor responses are invariant to air speed, as long as odor concentration is kept constant. This finding was true across a

>100-fold range of air speeds. Because odor hydrophobicity has been proposed to affect the air speed dependence of olfactory transduction, we tested a >1,000-fold range of hydrophobicity values, and found that ORN responses are invariant to air speed across this full range. These results have implications for the mechanisms of odor delivery to *Drosophila* ORNs. Our findings are also significant because flies have a limited ability to control air flow across their antennae, unlike terrestrial vertebrates which can control air flow within their nasal cavity. Thus, for the fly, invariance to air speed may be adaptive because it confers robustness to changing wind conditions.

Table of Contents

Abstract	iii
Table of Contents	v
List of Figures	vi
Acknowledgements	vii
CHAPTER 1: General Introduction	**1**
CHAPTER 2: Searching for central gustatory neurons in *Drosophila*	**3**
Introduction	3
Methods	9
Results	14
Calcium imaging	15
Photoactivable GFP	18
Visual screen to identify candidate Gal4 lines	24
Electrophysiological screening of candidate gustatory neurons	29
Physiological taste stimulation	32
Discussion	36
References	41
CHAPTER 3: Transduction in *Drosophila* olfactory receptor neurons is invariant to air speed	**44**
Introduction	44
Methods	50
Results	56
Independent control of air speed and odor concentration	56
Effect of air speed on olfactory receptor neuron responses	62
Discussion	73
References	80
CHAPTER 4: Conclusion	**84**

List of Figures

Figure 2.1: *Drosophila* taste receptors and associated neuropil. 4

Figure 2.2: Using the genetically encoded calcium indicator GCaMP to identify neurons in the *Drosophila* brain functionally connected to activation of GRNs. 17

Figure 2.3: Summary results of calcium imaging experiments. 19

Figure 2.4: Using photo activatable GFP to identify putative output neurons of the SOG. 22

Figure 2.5: Schematic of candidate Gal4 lines. 27

Figure 2.6: Whole-cell patch clamp recordings of candidate taste neuron cell bodies. 30

Figure 2.7: Schematic of preparation for patch clamp recordings of candidate taste neurons while delivering tastants to proboscis. 33

Figure 2.8: Tastant evoked responses of candidate taste neuron cell bodies. 34

Figure 3.1: Proposed mechanisms of air speed dependence in olfactory transduction. 45

Figure 3.2: Experimental setup. 57

Figure 3.3: Validation of odor delivery device using PID measurements. 60

Figure 3.4: Consistency of the odor pulse delivered to the PID. 63

Figure 3.5: ORN responses to linalool oxide depend on concentration but not air speed. 65

Figure 3.6: ORN responses to dibutyl sebacate depend on concentration but not air speed. 69

Figure 3.7: ORN responses to 1-propanol depend on concentration but not air speed. 70

Figure 3.8: ORN responses to 1-propanol are invariant to air speed at a range of low air speeds associated with natural *Drosophila* flight. 72

Figure 3.9: Dynamics of ORN responses to odor pulses of varying air speeds. 75

Figure 3.10: An example of a super-sustained ORN response. 78

Acknowledgements

Although this dissertation bears my name, it would not been possible without the help and support of countless others.

First and foremost, I'd like to thank my advisor Rachel Wilson for all that she has done for me in my graduate career. Anybody who has met Rachel will instantly recognize that she is a brilliant and articulate scientist, but what I and others in our lab have had the privilege of knowing is just how fantastic of a mentor she is. Her unwavering support and limitless compassion have been instrumental in seeing me through to the completion of my doctorate. Rachel always believed in me, even when I doubted myself. I was truly fortunate in having her as my mentor and as my friend.

I'd like to thank all the members of the Wilson lab for a stimulating and fun work environment. In particular I'd like to thank Vikas Bhandawat and Mehmet Fisek for keeping me company during long nights at the lab, Nathan Gouwens for his technical expertise and his ability and willingness to troubleshoot anything and everything, and Brendan Lehnert for working together with me to build our microscope and for always keeping an eye out for me.

I would like to thank the people who have served on my dissertation advisory committee over the years for their advice and expertise: John Assad, Dietmar Schmucker, Markus Meister, Gary Yellen, and Bob Datta. In particular I would like to thank Bernardo Sabatini for allowing me access to his microscopes during our pilot imaging experiments and for his technical advice during the construction of our 2-photon microscope.

I want to thank the Department and Defense and the Hertz foundation for the financial support they provided me during the course of my graduate studies.

I wish to thank my parents for their love and support throughout my life. Because of them, I have never been want for anything. They have worked hard and sacrificed much to ensure that I have had opportunities beyond that which they have had. I am extremely privileged to have been able to pursue that which I have wanted in life. This they have given to me, and I do not take it for granted.

Finally, I would like to thank my girlfriend and closest friend, Mary. Her love and companionship has mitigated the bad, punctuated the good, and inspired me to be a better person. Without her, none of this would have been possible. I know not what challenges I will face in life, but I know that I will face them with her by my side and that this will give me the strength I need to overcome them.

CHAPTER 1:

General Introduction

The detection of chemicals in the environment, or chemosensation, is essential for the survival and propagation of the individual and of the species. This oldest sense (in evolutionary terms) is used by organisms to locate nutrients and mates, and to avoid toxins and predators. The chemosensory systems of olfaction (volatile chemosensation) and gustation (contact chemosensation) are distinct from the other sensory systems in the qualitative heterogeneity of the stimuli that they have to detect.

Drosophila is an attractive model organism to use in the study of chemical senses. Flies are exquisitely sensitive chemical detectors and have many robust, well characterized gustatory and olfactory mediated behaviors that can be used to gain insight into the sensory perception of the fly. In addition, the number of cells underlying sensory systems in flies is relative small, on the order of hundreds of neurons. As in other relatively simple invertebrate nervous systems, many neurons are uniquely identifiable in *Drosophila.* In *Drosophila* we have a variety of genetic tools to label and manipulate the neural activity of these identifiable neurons. This in conjunction with our ability to make *in vivo* electrophysiological recordings from single cells in awake, behaving flies makes it possible to gain insight into general principles of sensory processing.

In this dissertation I present two separate studies in *Drosophila* chemosensation. In Chapter 2, I describe a project focused on the identification of central gustatory neurons. In Chapter 3, I describe a study looking at the effect of air speed on olfactory transduction. These two studies use different techniques, different approaches, and have very different aims. They are united by the use of *Drosophila* as model organism in

studying chemical sensation. Both studies rely on the concept of identified neurons and on our ability to make measurements from the same neuron again and again in different flies. Both studies faced significant technical hurdles and required substantial amounts of engineering to present chemical stimuli in which the relevant parameters were under precise control.

Each study is motivated by and rests upon a substantial foundation of previous literature. However, because the background literature of the two projects is very distinct from one another, the literature germane to each study is presented at the beginning of each respective chapter.

CHAPTER 2:

Searching for central gustatory neurons in *Drosophila*

INTRODUCTION

Motivation for developing strategies to establish functional connectivity in the Drosophila brain

Over the course of the last decade *Drosophila melanogaster* has emerged as a powerful model organism in systems neuroscience. Technological advances have made it possible to monitor the activity of single neurons in the fruit fly brain through electrophysiology (Wilson, Turner et al. 2004) or of populations of neurons through functional imaging (Fiala, Spall et al. 2002; Ng, Roorda et al. 2002; Wang, Wong et al. 2003). These techniques used in combination with the Gal4/UAS enhancer trap system (Brand and Perrimon 1993) have made it feasible to complete functional studies of identified groups of neurons with known connectivity.

Despite their genetic advantages, systems neuroscience studies in *Drosophila* are greatly inhibited by our ignorance concerning the functional organization of central circuits in the fly. This has prohibited identification of central neurons involved in various sensations and restricted the scope of inquiry to the two systems with good anatomical organization: vision and olfaction. In these modalities, the anatomy is so highly structured that morphology alone is sufficient to establish connectivity between specific peripheral sensory neurons and higher-order central neurons (Figure 2.1A). This has greatly facilitated both the study and interpretation of central representations in these sensory systems (Olsen, Bhandawat et al. 2007).

Figure 2.1: *Drosophila* taste receptors and associated neuropil. *A*: schematic of anterior view of *Drosophila* brain. AL: antennal lobes (olfactory neuropil). SOG: sub-esophageal ganglion (gustatory neuropil). LN: labellar nerve, nerve which houses the axons of peripheral gustatory receptor neurons (GRNs) of the proboscis. Inserts are confocal images of olfactory and gustatory neuropil taken using a neuropil stain (nc82). Note the clear compartmental organization of olfactory neuropil as compared to the gustatory neuropil. Scale bars represent 20μm. *B*: location and morphology of gustatory organs in *Drosophila*. Insets are scanning electron micrographs of the proboscis, wing, and leg. Arrows indicate gustatory sensilla. Scale bars represent 50μm. Adapted from Ishimoto and Tanimura 2004.

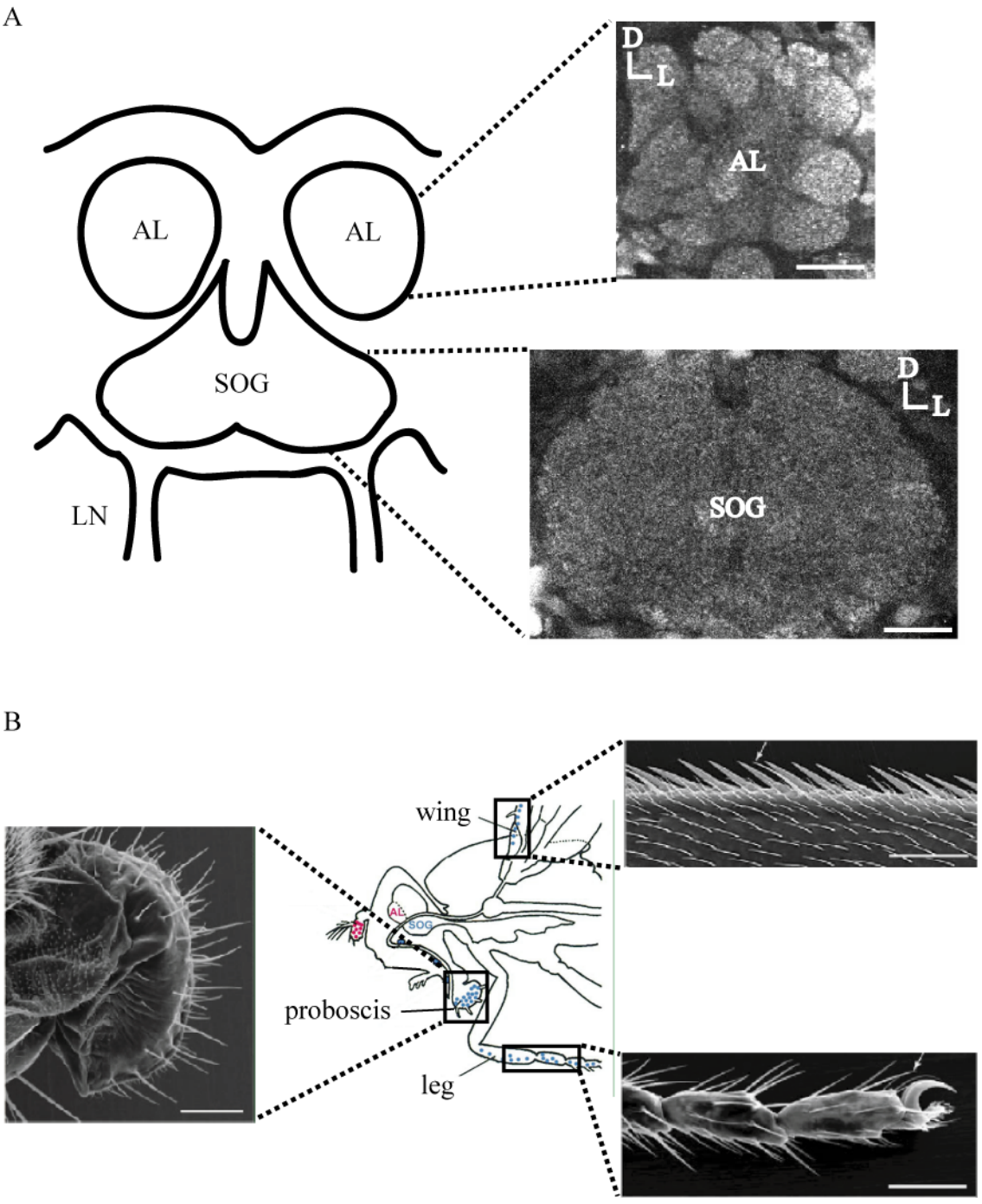

Figure 2.1: (Continued)

To date, no one has found central neurons implicated in other modalities in *Drosophila*. The neuropil of other sensory systems is relatively disorganized (Fig 2.1A) and thus is not as amenable to sole use of anatomical techniques in establishing connectivity. Trans-synaptic tracers used in mammalian preparations (Horowitz, Montmayeur et al. 1999; Wickersham, Lyon et al. 2007) are ineffectual in *Drosophila* (Morante and Desplan 2004). It is also not uncommon in the *Drosophila* brain for cell bodies to be located great distances away from their neurites, making it impossible to infer connectivity based solely on somatic proximity to the neuropil of interest.

If our knowledge of sensory processing is to be advanced in these other modalities, a standard strategy must be developed to establish functional connectivity. In this project, we used calcium imaging in conjunction with photo-activatable GFP (PA-GFP) in an attempt to identify and characterize higher-order gustatory neurons in *Drosophila*.

Peripheral taste processing in Drosophila

Much is known about gustatory transduction and coding at the level of peripheral receptor neurons in *Drosophila*. There are approximately 660 gustatory receptor neurons (GRNs) in adult *Drosophila* (Stocker 1994). GRNs are housed in protrusions of the cuticle called sensilla (Fig 2.1B, arrows). These gustatory sensilla are innervated by two to four gustatory receptor neurons and by a single mechanosensory neuron (Falk, Bleiser-Avivi et al. 1976). The dendrites of GRNs extend to the tip of the sensilla where they are exposed to the external environment via a single pore.

These gustatory sensilla are located on the proboscis, legs, and wings (Fig 2.1B). In this project, we focused on the proboscis, the insect analog of the tongue. The taste receptive fields of the sensilla located on the proboscis have been extensively characterized electrophysiologically (Hiroi, Marion-Poll et al. 2002; Hiroi, Meunier et al. 2004). These recordings have demonstrated that GRNs are tuned to different tastes: each neuron responds best to either sugar, water, low concentrations of salts, or high concentrations of salt and bitter compounds.

The taste receptor gene family in *Drosophila* was recently identified (Clyne, Warr et al. 2000; Dunipace, Meister et al. 2001; Scott, Brady et al. 2001) by BLAST searches with *Drosophila* odorant receptor sequences. Expression analysis of several of these genes has subsequently confirmed their expression in the GRNs of the proboscis and legs. The expression profiles of *Gr* genes in GRNs are complex (Thorne, Chromey et al. 2004; Wang, Singhvi et al. 2004). Some *Gr* genes are restricted in expression to a few neurons in one or two taste organs, whereas others are expressed in a majority of GRNs in all taste organs.

The function of these GRN types has been examined by genetically-inactivating specific sets of GRNs. This has been accomplished by expressing diphtheria or tetanus toxin under the control of various *Gr* drivers (Thorne, Chromey et al. 2004). It was found that flies lacking *Gr66a*-expressing neurons had reduced sensitivity to bitter compounds but not sweet ones, while flies lacking *Gr5a*-expressing neurons had the opposite phenotype. The main conclusion from these studies was that GRNs can broadly be divided into two functional groups, one required for detection of sugars and another for the detection of aversive stimuli.

GRN projections into the Drosophila brain

GRNs from the proboscis project to the subesophageal ganglion (SOG) in the brain. As GRNs are expressed in various organs and express different combinations of gustatory receptors, it is natural to ask whether there is segregation of projections based on either position or taste quality.

Golgi stains of GRNs have revealed a gross topographic map of organ location in the SOG (Shanbhag and Singh 1992; Rajashekhar and Singh 1994). Projections of GRNs internal to the mouthparts are anterior to those from the proboscis, which are in turn anterior to those from the legs. These stains have also been used to construct rudimentary classifications of types of labellar sensory projections based on morphology. It should be noted that these different types of projections often overlap with each other in the SOG, and thus are not nearly as well delineated as those in the olfactory system.

Projections of GRNs seem to also be crudely segregated by taste quality. GRNs expressing *Gr5a*, known from functional studies to mediate sugar detection, project to a somewhat different area in the SOG than those which express *Gr66a*, known to mediate detection of bitter compounds (Thorne, Chromey et al. 2004). It appears from these studies that rudimentary maps of position and taste quality exist in the fly brain.

General aims and scope of our project

To date no central neurons involved in gustation have been reported in *Drosophila*, except for one study characterizing a motor neuron involved in the proboscis extension reflex (Gordon and Scott 2009). The primary aim of this project was to identify and characterize higher-order gustatory neurons.

Our strategy for achieving this goal was to take complementary functional and anatomical approaches. We used calcium imaging to screen for cells responding to stimulation of GRNs along with photo-activation of photo-activatable GFP (PA-GFP) to localize the cell bodies of neurons innervating the SOG. Based on the information we gained from these imaging experiments, we identified some promising Gal4 lines that labeled candidate gustatory neurons. Finally, we made recordings from these putative gustatory neurons while simultaneously stimulating the proboscis with tastants.

METHODS

Fly stocks

In order to perform the imaging experiments, we used the Gal4/UAS-system (Brand and Perrimon 1993) to direct expression of the calcium sensor GCaMP (Nakai, Ohkura et al. 2001) or photoactivatable green fluorescent protein (Patterson and Lippincott-Schwartz 2002; Datta, Vasconcelos et al. 2008) to all cholinergic neurons. Cholinergic neurons were selected because acetylcholine represents the major excitatory neurotransmitter of the Drosophila brain. Expression was localized to putative cholinergic neurons using a Gal4 transgene which incorporates the promoter for the choline acetyltransferase (ChaT) gene (Yasuyama and Salvaterra 1999). This resulted in generation of *ChaT-Gal4;UAS-GCaMP1.3* and *ChaT-Gal4; UAS-PA-GFP* flies. *UAS-GCaMP* and *UAS-PA-GFP* stocks were kindly provided by Richard Axel and Bob Datta. *ChaT-Gal4* was obtained from Bloomington.

Electrophysiological recordings from GFP positive cells in Chapter 2 were made from *a125-Gal4, UAS-CD8GFP* flies, *a159-Gal4, UAS-CD8GFP* flies (gifted from Julie Simpson), and *c600-Gal4, UAS-CD8GFP* flies (www.Fly-Trap.org).

All experiments were performed on adult female flies, 2-5 days after eclosion. Flies were reared on standard cornmeal agar medium.

Isolated fly head preparation

All experiments (save those presented in Figure 2.8, see Intact fly preparation and tastant delivery below) were completed in a head-only preparation. Flies were anesthetized in a glass vial on ice just until movement stopped (~30s). Flies were then decapitated. Heads were transferred to a small glass well filled with saline as previously described (Wilson and Laurent 2005). Using forceps, an incision was made at the ventral edge of the head capsule around the proboscis. The proboscis was then dissected off gently, taking care to preserve the labellar nerve. The antennae were then dissected off as well, taking care to remove the antennal nerves. The remainder of the cuticle on the anterior surface of the head was then peeled off, from the proboscis to the ocelli on the dorsal edge of the head capsule. Fat and air sacs anterior to the fly brain were removed. For electrophysiological experiments, the perineural sheath was gently picked away from the SOG. This sheath was left intact for imaging experiments, as it didn't occlude optic access to the brain. This dissected head capsule was then transferred carefully to a stage where it was secured via two modified glass slides pressing down on the eyes.

Imaging and photo-activation

Imaging and photoactivation was done with a custom 2-photon laser-scanning microscope as previously described (Carter and Sabatini 2004) built with great assistance from Rachel Wilson and fellow graduate student Brendan Lehnert. Bernardo Sabatini provided invaluable technical advice in this endeavor.

A mode-locked Ti: sapphire laser (Mai Tai, Spectra Physics) tuned to 925nm was directed to a system of galvanometric scan mirrors (6210H, 6mm, Cambridge Technology) and focused through a modified microscope (BX51, Olympus) onto the fly brain using a 20 x 0.95NA water immersion lens (XLUMPlanFl, Olympus). The epi-collected florescence was bandpass filtered (FF01-534/30-50, Semrock) and detected with gallium arsenide photo multiplier tubes (H7422P-40MOD, Hamamatsu). Analog output from photo multipliers was amplified (SR570, Stanford Research Systems) then acquired via ScanImage (Pologruto, Sabatini et al. 2003) through a data acquisition board (PCI-6110, National Instruments). Time series (Figure 2.2) consisted of forty frames of 256x256 pixel images, captured at a scan speed of 2ms/line or 512ms/frame. Z-stacks (Fig 2.4) were collected as 512x512 pixel images at a scan speed of 4ms/line or 2s/frame.

Photo-activation (Figure 2.4) was accomplished by using the imaging software to center on the region of desired photoactivation, re-tuning the laser to 710nm, then scanning over the brain tissue ten times (128x128 pixels, 4ms/line) with an inter-scan interval of one minute. We allowed ten minutes to elapse after photo-activation to permit diffusion of photoactivated GFP before imaging again at 925nm.

Stimulation of labellar Nerve

During electrophysiological recordings of candidate gustatory neurons (Figure 2.6), the labellar nerve was drawn into a saline-filled suction electrode and a brief pulse (100us) of current (1uA) was passed through the nerve using a stimulus isolator (Iso-flex, AMPI). Evoked EPSCs were verified to be mediated through synaptic transmission via addition of 50uM of cadmium chloride into the saline. This concentration of bath-applied cadmium chloride has been verified to block acetylcholine release from olfactory receptor neuron axon terminals (Kazama and Wilson, 2008). After wash out of cadmium, sometimes 50uM mecamylamine (Sigma) was added to the saline to test if evoked EPSCs were mediated by nicotinic acetylcholine receptors.

During imaging experiments (Figure 2.2), a train of 200 pulses was used instead of just one pulse to elicit the stronger responses necessary for detection with a genetically encoded calcium indicator. This train of pulses was delivered over the course of 2 seconds with an inter pulse interval of 10ms.

Electrophysiology

Whole-cell patch-clamp recordings from candidate gustatory neurons were obtained from GFP positive neurons in three strains: (1) *a125-Gal4,UAS-CD8GFP*, (2) *a159-Gal4,UAS-CD8GFP*, and (3) *c600-Gal4,UAS-CD8GFP*. Fly brains were mounted underneath an upright compound microscope (Olympus BX-51) with a fluorescence attachment and visualized with a 40x, 0.8 NA water immersion lens (LUMPlanFL/IR, Olympus). Patch-clamp electrodes were filled with standard internal solution as described previously (Wilson, Turner et al. 2004). Signals were acquired on an A-M Systems

Model 2400 amplifier and low-pass filtered at 5 kHz with a LPF202A signal conditioner (Warner Instruments) before digitization at 10 kHz. Digitized signals were acquired using custom routines written in IgorPro (Wavemetrics) through a PCI-6251 data acquisition board (National Instruments).

Intact fly preparation and tastant delivery

In experiments using tastants (Figure 2.8), flies were prepared for *in vivo* recording, as distinct from the isolated head preparation detailed above. Flies were anesthetized in a glass vial on ice just until movement stopped (~30s). They were then gently inserted into a hole in a horizontal piece of aluminum foil positioned within a larger horizonal platform. Small drops of wax were used to secure the fly in the hole, taking care to align the plane of the foil with the posterior edge of the fly's head capsule. The antennae were positioned on the dorsal (upper) side of the foil whereas the palps and the proboscis were positioned on the ventral (lower) side. This alignment was necessary for physical access to the candidate gustatory neurons. The palps were epoxied to a piece of human hair waxed to the ventral side of the foil and positioned orthogonally to the palps and proboscis (Figure 2.7). This permitted extension of the proboscis along its long axis, away from the plane of the foil, by manipulating the position of the hair. This was done as to permit physical access of tastant to the proboscis.

The dorsal side of the foil was then bathed in saline while the ventral side (including the maxillary palps and the proboscis) remained dry. It was essential that the proboscis did not come into contact with the saline, as we observed that this desensitized it to subsequent tastants. Once the dorsal side of the foil was bathed in saline, the

antennae were dissected away, as well as the anterior cuticle of the head capsule between the eyes and from the proboscis to the ocelli. Fat and air sacs anterior to the brain were moved and the perineural sheath surrounding the candidate neurons was gently picked away. Muscles surrounding the proboscis and the esophagus were dissected away, taking care not to damage the labellar nerve. (If these were kept intact, the movement of the brain was too large to permit stable recordings.)

The fly was then mounted underneath the upright compound microscope. A video camera mounted underneath the fly (Unibrain Fire-I BBW 1.3 Camera, equipped with an 8mm telephoto lens, 1394 Store) was used to position a glass pipette filled with one of four tastants (distilled water, 1M trehalose in water, 1mM quinine in water, or 50mM NaCl in water) mounted on a bending piezoelectric bending actuator (D220-A4-103YB, Piezo Systems Inc.) near the proboscis. A step pulse of two seconds was delivered to the piezo while the camera was used to visually verify that this corresponded to delivery of the tastant to the proboscis. The ventral side of the aluminum foil was colored black using a Sharpie pen to give maximal visual contrast between the foil and the proboscis, because this improved positioning of the pipette.

RESULTS

The overall goal of this project was to identify and characterize higher-order gustatory neurons in *Drosophila melanogaster*. Outside of one study characterizing a motor neuron involved in the proboscis extension reflex (Gordon and Scott 2009), no study to date has described central gustatory neurons in *Drosophila*. Thus our first aim was to identify putative gustatory neurons in the *Drosophila* brain. Our strategy for

tackling this problem involved complementary functional and anatomical approaches. We used calcium imaging to screen for cells responding to stimulation of peripheral gustatory neurons, and we used photo-activatable GFP (PA-GFP) to localize the cell bodies of neurons innervating the neuropil associated with gustation, the SOG. For these experiments, we built our own custom two photon laser microscope (see Methods).

Throughout our imaging experiments, we used the known connectivity and selectivity of the olfactory sensory system in *Drosophila* as a positive control for our protocols. This allowed us to optimize both our stimulus and imaging parameters to maximize the likelihood of detecting putative central gustatory neurons.

Calcium imaging

As most depolarizing electric signals in neurons are accompanied by an influx of calcium into the cell, calcium can be used as a proxy measure of neural activity. Broadly speaking, there are two classes of calcium indicators: small chemical indicators derived from calcium chelators and large genetic indicators derived from calcium binding proteins. The smaller chemical indicators (e.g. fura-2, Oregon Green BAPTA) generally have faster dynamics and greater sensitivity compared to genetic indicators (e.g. GCaMP). However, the great advantage of genetic indicators is our ability to restrict their expression to specific groups of cells.

In pilot experiments, we tried bulk loading of cell permeable variants of chemical indicators into the *Drosophila* brain. However, we could not get consistent loading and responsiveness of known central olfactory neurons to strong stimulation of peripheral olfactory neurons. For this reason, the calcium imaging experiments described below

were completed with GCaMP (Nakai, Ohkura et al. 2001), a genetically encoded calcium indicator derived from the protein calmodulin. Specifically, we used the Gal4/UAS-system (Brand and Perrimon 1993) to direct expression of GCaMP to all cholinergic neurons. As acetylcholine is the major excitatory neurotransmitter in the *Drosophila* central nervous system, we assumed it to be the neurotransmitter mediating transmission of gustatory information. Acetylcholine also mediates transmission of olfactory information, making it possible for us to use the olfactory system as a positive control.

To functionally identify potential central gustatory neurons, we used calcium imaging in conjunction with stimulation of GRNs. We attempted to use physiological taste stimulation of GRNs, but this was problematic as the proboscis was submerged in saline during our initial imaging experiments. This seemed to desensitize GRNs to subsequent tastants. For this reason, we settled upon direct electrical stimulation of the labellar nerve, the nerve housing the axons of GRNs. In addition to housing GRN axons, the labellar nerve contains the axons of olfactory receptor neurons housed in the maxillary palps, which is an auxillary olfactory organ. (The labellar nerve also contains the axons of mechanosensitive neurons located in the palps and the proboscis.) Thus, because the labellar nerve contains olfactory receptor neuron axons, it was possible for us to optimize our nerve stimulation protocol using the known connectivity of these neurons to secondary olfactory neurons immediately dorsal to the antennal lobe. We adjusted the parameters of nerve stimulation to maximize the signal obtained from these central olfactory neurons directly post-synaptic to peripheral olfactory receptor neurons (Figure 2.2A). We then used this same nerve stimulation protocol while imaging cell bodies in and around the SOG, where we found many responsive neurons (Figure 2.2B).

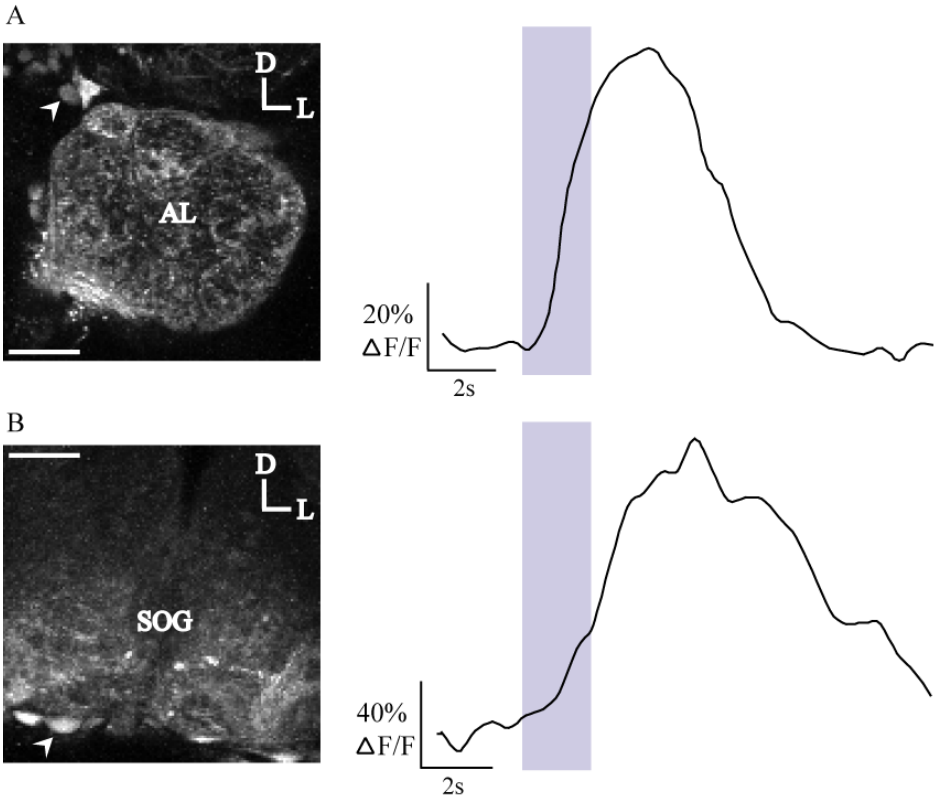

Figure 2.2: Using the genetically encoded calcium indicator GCaMP to identify neurons in the *Drosophila* brain functionally connected to activation of GRNs. *A*: Response of a second-order olfactory neuron (indicated by arrow in an image of resting fluorescence) to stimulation of labellar nerve. Because this nerve contains axons of primary olfactory receptor neurons in the maxillary palps, it is directly presynaptic to some second-order olfactory neurons. *B*: Response of candidate central gustatory neuron (indicated by arrow) to stimulation of the labellar nerve. Because this nerve contains the axons of GRNs, it should be directly presynaptic to all second-order gustatory neurons. Nerve stimulation duration in gray. Images on the left represent resting fluorescence in *ChaT-Gal4;UAS-GCaMP1.3* flies. AL: antennal lobes. SOG: sub-esophageal ganglion.

Over the course of many experiments, we started to note that certain regions seemed to contain a high density of neurons that responded to labellar nerve stimulation consistently. Specifically, the region immediately dorsal to the anterior most portion of the SOG contained many cell bodies that seemed to respond to labellar nerve stimulation in almost every preparation (Figure 2.3). The region lateral to the SOG also contained some responsive neurons, but these responses were not as consistent as those immediately dorsal to the anterior SOG. A few neurons ventral to the SOG responded to our nerve stimulus protocol, but not many.

In summary, our functional imaging experiments suggest that a great number of cells dorsal, lateral, and ventral to the SOG respond to stimulation of the labellar nerve. The greatest concentration of responses comes from cells located directly dorsal to the most anterior portion of the SOG neuropil. Responsive cells are candidates for second-order gustatory neurons (i.e., neurons directly postsynaptic to GRN axons). However, based solely on calcium responses to stimulation of the labellar nerve, it is not possible to conclude that a neuron is directly postsynaptic to GRNs, because these neurons may be receive only indirect excitation from GRNs. Alternatively, these neurons may be postsynaptic to the maxillary palp, or may be postsynaptic to mechanosensory neurons.

Photoactivable GFP

Next, we conducted a series of anatomical experiments with photoactivatable GFP (Patterson and Lippincott-Schwartz 2002). This is a variant of GFP that increases fluorescence a hundred fold when exposed to a particular wavelength of light. This photoactivated GFP readily diffuses throughout all a neuron's processes. Thus, one can

Figure 2.3: Summary results of calcium imaging experiments. Schematics of four coronal optical sections of the fly brain, indicating the response strength of cell bodies located at these positions to simulation of the labellar nerve. Only cell bodies contralateral to labellar nerve are schematized as responding. AL: antennal lobes. SOG: sub-esophageal ganglion.

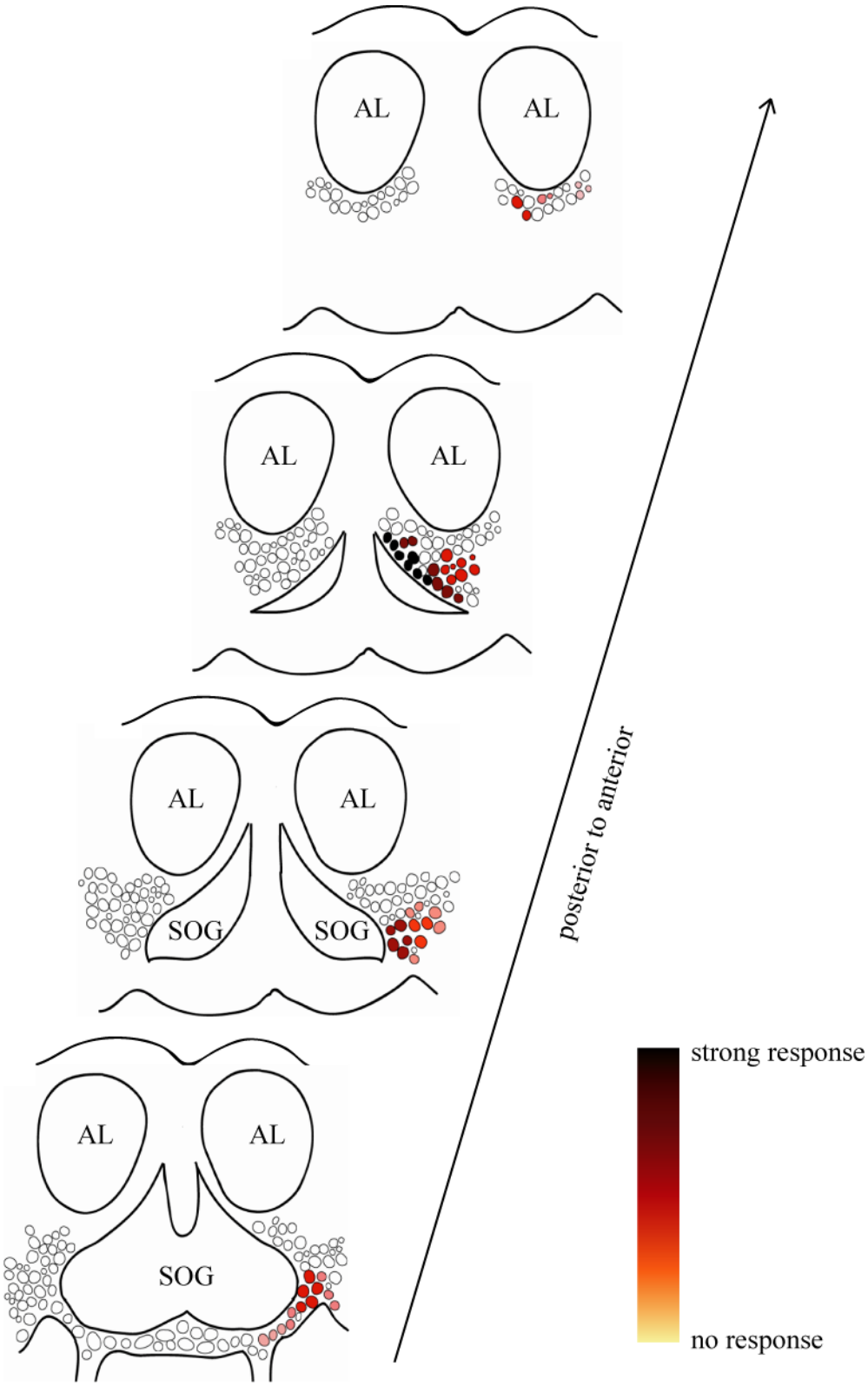

Figure 2.3: (Continued)

photoactivate in a cell body to find a neuron's axons and dendrites, or alternatively, one can photoactivate neuropil in a region of interest to find where the corresponding cell bodies are located.

The aim of these experiments with PA-GFP was to identify putative output neurons of the SOG. These neurons would have processes in the SOG proper and also project out of the SOG. All experiments were conducted in flies harboring a *UAS-PA-GFP* transgene expressed under the control of the *ChaT-Gal4* driver, putatively labeling all cholinergic neurons in the fly brain.

Again, we initially used the olfactory system as a positive control to optimize our activation protocol. We found that a few short strong bursts of laser delivered with an inter pulse interval of one minute gave the best results. We could easily use PA-GFP to trace out the neural processes of a local neuron in the olfactory system (Figure 2.4A) by photoactivating a single cell body.

We then used this stimulus protocol to photoactivate a large portion of the SOG neuropil, with the aim of finding the cell bodies that send dendrites into this neuropil. When we photoactivated GFP in a large fraction of the SOG neuropil, we saw that many cell bodies in the immediate vicinity of SOG were labeled. This protocol also uncovered a neural tract that seemed to connect the SOG to the mushroom bodies (Figure 2.4B), a region of the *Drosophila* brain implicated in higher order sensory integration and memory. This seemed to be a putative output tract of the gustatory neuropil.

To further explore this putative output tract, we performed a series of experiments specifically photactivating this fiber bundle. We found that fibers of this tract seem to innervate the anterior dorsal SOG neuropil, and the posterior antennal lobe neuropil, as

Figure 2.4: Using photo activatable GFP to identify putative output neurons of the SOG. Images are of *ChaT-Gal4;UAS-PA-GFP* flies before (left) and after (right) photoactivation of areas delineated by red boxes. *A*: photoactivation of the cell body of an olfactory local interneuron labels the cell's processes in the antennal lobe. *B*: photoactivation of large region of SOG neuropil reveals a putative output tract connecting the SOG to other brain regions. *C*: photoactivation of this putative gustatory output tract labels cell bodies ventral to the SOG, along with cell bodies lateral to the antennal lobe and immediately dorsal to the antennal nerve. AL: antennal lobes. AN: antennal nerve. SOG: sub-esophageal ganglion. Scale bars represent 20μm.

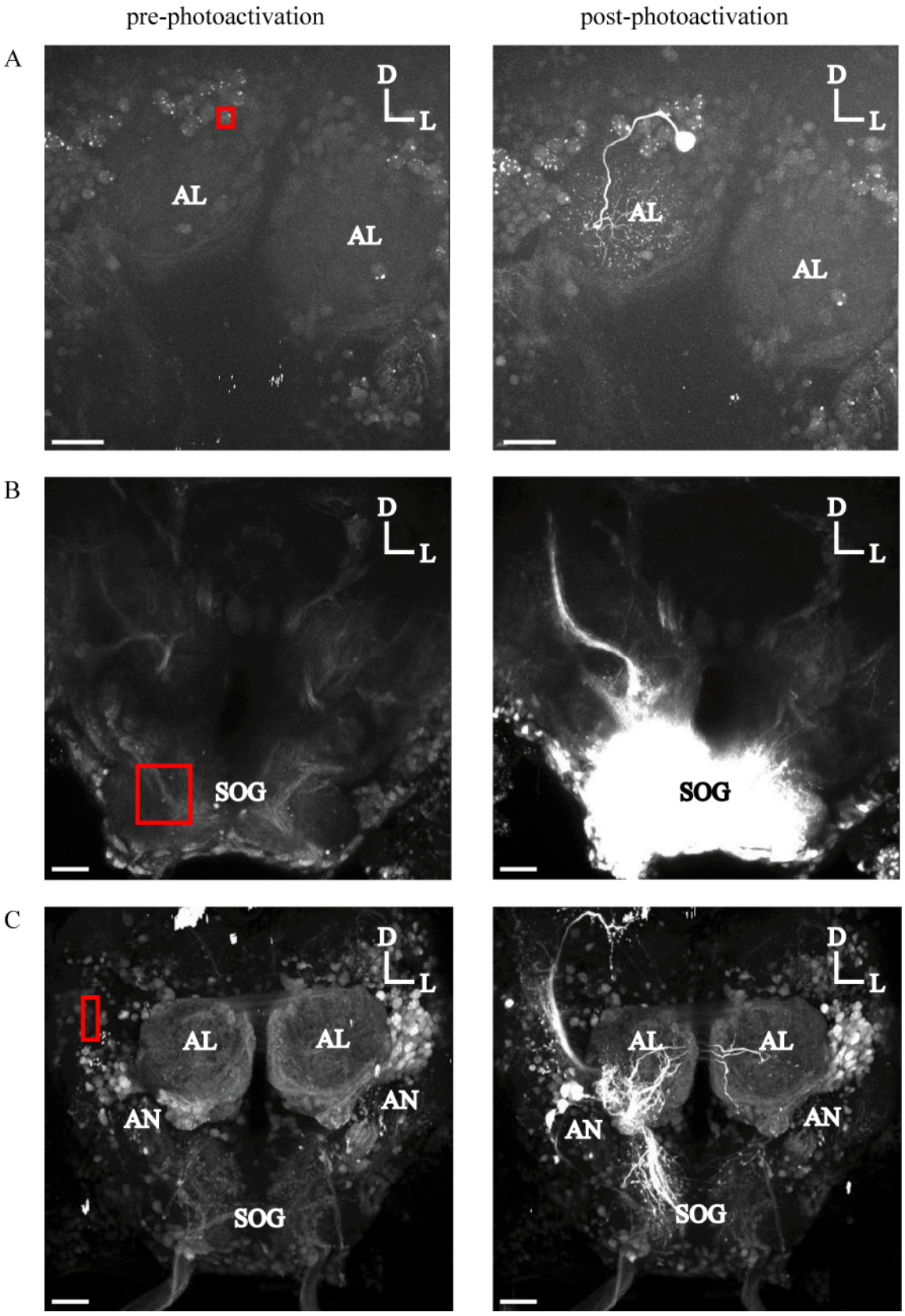

Figure 2.4: (Continued)

well as the mushroom bodies and an additional higher-order brain region (the lateral protocerebrum). In addition, one group of cell bodies ventral to the SOG and another group lateral to the antennal lobe and immediately dorsal to the antennal nerve seemed to be labeled by photoactivating this fiber tract (Figure 2.4C).

In summary, our PA-GFP experiments confirmed that a large number of cells located in the immediate vicinity of the SOG send processes into the SOG neuropil. We also found a putative output tract connecting the SOG to two higher brain regions. Two groups of cells, one immediately dorsal to the antennal nerve and one ventral to the SOG, seem to send processes through this tract.

The potential value of these PA-GFP experiments, combined with the calcium imaging experiments described above, was to guide our visual screen of candidate Gal4 lines. Based on the PA-GFP and calcium imaging results, we knew that we should be screening for neurons having cell bodies in the immediate vicinity of the SOG. We were also particularly interested in screening for Gal4 lines for neurons that appeared to innervate the putative output tract we had discovered.

Visual screen to identify candidate Gal4 lines

The imaging experiments described above provided us with a functional and anatomical map of gustatory processing in *Drosophila*. We used this information to visually screen through hundreds of Gal4 lines in order to find ones that labeled putative gustatory neurons. This Gal4 screen was a critical step because, in the absence of a Gal4 line, it is very difficult to make targeted electrophysiological recordings from specific neuron types in the *Drosophila* brain.

In our screen, candidate Gal4 lines were evaluated on the basis of several criteria. In order to be worth pursuing, a Gal4 line had to satisfy all these criteria:

- Candidate Gal4 lines had to be sparse enough to unambiguously identify the neuron of interest across different preparations.
- Candidate Gal4 lines had to label neurons that had neural processes in the SOG.
- Candidate neurons had to have cell bodies either in the region dorsal to the anterior portion of the SOG, found by calcium imaging to contain cells extremely responsive to stimulation of the labellar nerve, or else to have cell bodies located immediately dorsal to the antennal nerve or ventral to the SOG, regions shown by PA-GFP experiments to house cell bodies that sent processes through the putative output tract of the SOG.
- Finally, candidate neurons had to be located in positions amenable to whole-cell patch clamp recordings.

We performed a visual screen of several hundred Gal4 lines with these criteria in mind. These Gal4 lines came from several sources:

- Julie Simpson's collection of unpublished enhancer-trap and promoter-fusion Gal4 lines (Janelia Farm Research Campus). All these lines had been previously imaged by the Janelia Farm imaging core, and the confocal stacks were made available to us by kind consent of Dr. Simpson.
- The FlyTrap project (www.fly-trap.org, a public collection hosted by the University of Edinburgh). All these lines had been previously imaged, although the available images were often poor, and we ended up needed to re-cross and re-image many candidates to clarify the anatomy of the Gal4-expressing neurons.

- Kristin Scott's collection (UC Berkeley), published in Gordon and Scott 2009. None of these lines were imaged, so we re-crossed and re-imaged them all to perform our visual screen. All of these 61 these lines had been identified by the Scott lab based on a behavioral screen. Namely, all of them, when crossed with a genetically-encoded loss-of-function transgene (a potassium channel, *UAS-Kir2.1*), had produced a defect in the fly's innate proboscis extension response to sucrose stimulation of GRNs on the proboscis. Unfortunately, although all these lines had produced a defective behavior, most of them did not specifically label neurons having processes in the SOG.

In the course of this screen, we found four promising candidate Gal4 lines (Figure 2.5). Two lines, *c600-Gal4* and *a159-Gal4*, labeled neurons with cell bodies located dorsal to the anterior most portion of the SOG neuropil. This was the region revealed by calcium imaging to contain neurons that most consistently responded to stimulation of the labellar nerve. The *c600-Gal4* line labeled a neuron that innervated the posterior portion of the SOG, whereas the *a159-Gal4* line labeled a neuron that innervated the dorsal, anterior portion of the SOG. The two other candidate Gal4 lines labeled neurons with cell bodies dorsal to the antennal nerve (*a125-Gal4*) and ventral to the SOG (*T2-Gal4*), regions known to contain cells which sent processes through the putative output tract of the SOG. In both cases, labeled neurites were present in the SOG neuropil. Importantly, imaging the candidate neuron labeled by *T2-Gal4* revealed that it had processes both in the SOG and in the putative output tract of the SOG, making it a good candidate for a principal central gustatory neuron.

Figure 2.5: Schematic of candidate Gal4 lines. Shown in different colors are the locations of the cell bodies and innervation patterns of our four most interesting candidate lines relative to gustatory and olfactory neuropils (SOG and AL). All lines labeled one pair of candidate neurons whose neurites were bilaterally symmetric to one another. Only one neuron per line is schematized for clarity. These lines were identified based on a visual screen, followed by whole-cell patch-clamp recording while stimulating the nerve containing GRN axons. The candidate neuron labeled by *T2-Gal4* sends neurites to the SOG, and also out of the SOG via the putative gustatory output tract. All other candidates contain only neurites local to the SOG. AL: antennae lobe. SOG: sub-esophageal ganglion. LN: labellar nerve.

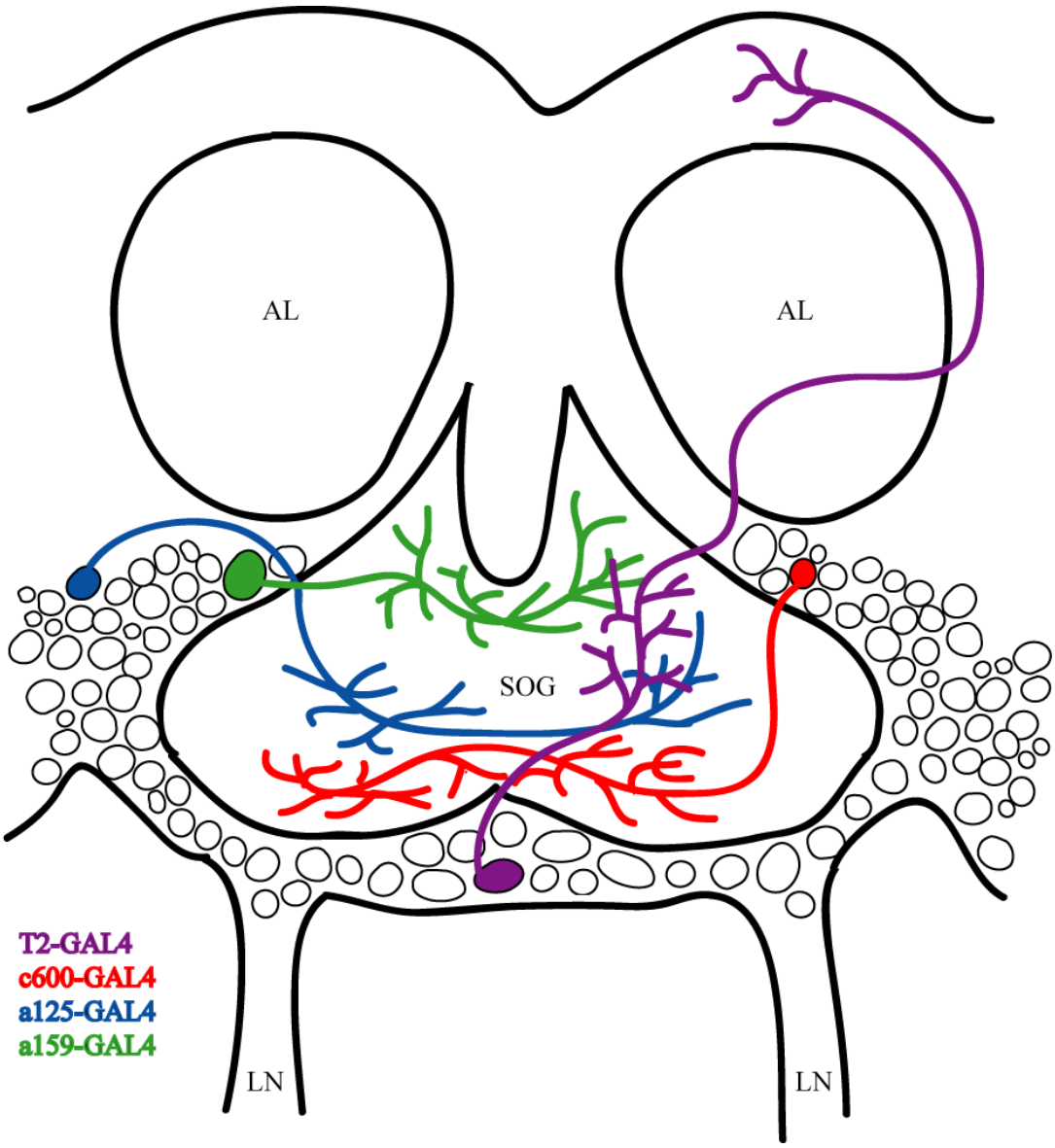

Figure 2.5: (Continued)

Electrophysiological screening of candidate gustatory neurons

Next, we investigated whether any of our candidate gustatory neurons were directly postsynaptic to GRNs. We made whole-cell patch clamp recordings from candidate neurons in an isolated brain preparation, while simultaneously exciting GRN axons via electrical stimulation of the severed labellar nerve.

We found that stimulation of labellar nerve axons elicited fast, reliable EPSCs with a 2-3 ms latency in neurons labeled by two of our candidate Gal4 lines: *c600-Gal4* (Figure 2.6A) and *a159-Gal4* (Figure 2.6B). These EPSCs disappeared in the presence of either cadmium or mecamylamine, an antagonist of nicotinic acetylcholine receptors. Taken together, these results imply that both of these Gal4 lines label neurons that are postsynaptic to cholinergic neurons with axons housed in the labellar nerve. However, this result does not necessarily indicate that these neurons are postsynaptic to GRNs, because they might instead be postsynaptic to non-GRN neurons in the nerve (olfactory receptor neurons or mechanosensory neurons).

Labellar nerve stimulation elicited relatively small, slow EPSCs in the candidate neuron labeled by the *a125-Gal4* line (Figure 2.6C). These EPSCs were also abolished in the presence of mecamylamine. These experiments suggested that the candidate gustatory neuron labeled by *a125-Gal4* was indirectly coupled to activation of neurons with axons in the labellar nerve.

We were unfortunately unable to make recordings from candidate neurons labeled by *T2-Gal4* while stimulating the labellar nerve, due to their position. These cell bodies are located in the extreme ventral region of the SOG, and we found that desheathing

Figure 2.6: Whole-cell patch clamp recordings of candidate taste neuron cell bodies. These recordings show responses to electrical stimulation of the labellar nerve, which contains GRN axons. *A*: EPSCs recorded in a candidate taste neuron labeled by *c600-Gal4* in response to labellar nerve stimulation. Several EPSCs are overlaid to show trial-to-trial variability. Mecamylamine (50μM) and cadmium (50μM) both block this response. Arrow indicates stimulus artifact. Below raw traces is a summary of the of the EPSC magnitude over the course of one experiment under different pharmacological conditions. *B*: same as *A*, but for a candidate taste neuron labeled by *a159-Gal4*. *C*: same as in *A* and *B*, but for a candidate taste neuron labeled by *a125-Gal4*. Note the compressed time scale of this last EPSC as compared to the other two.

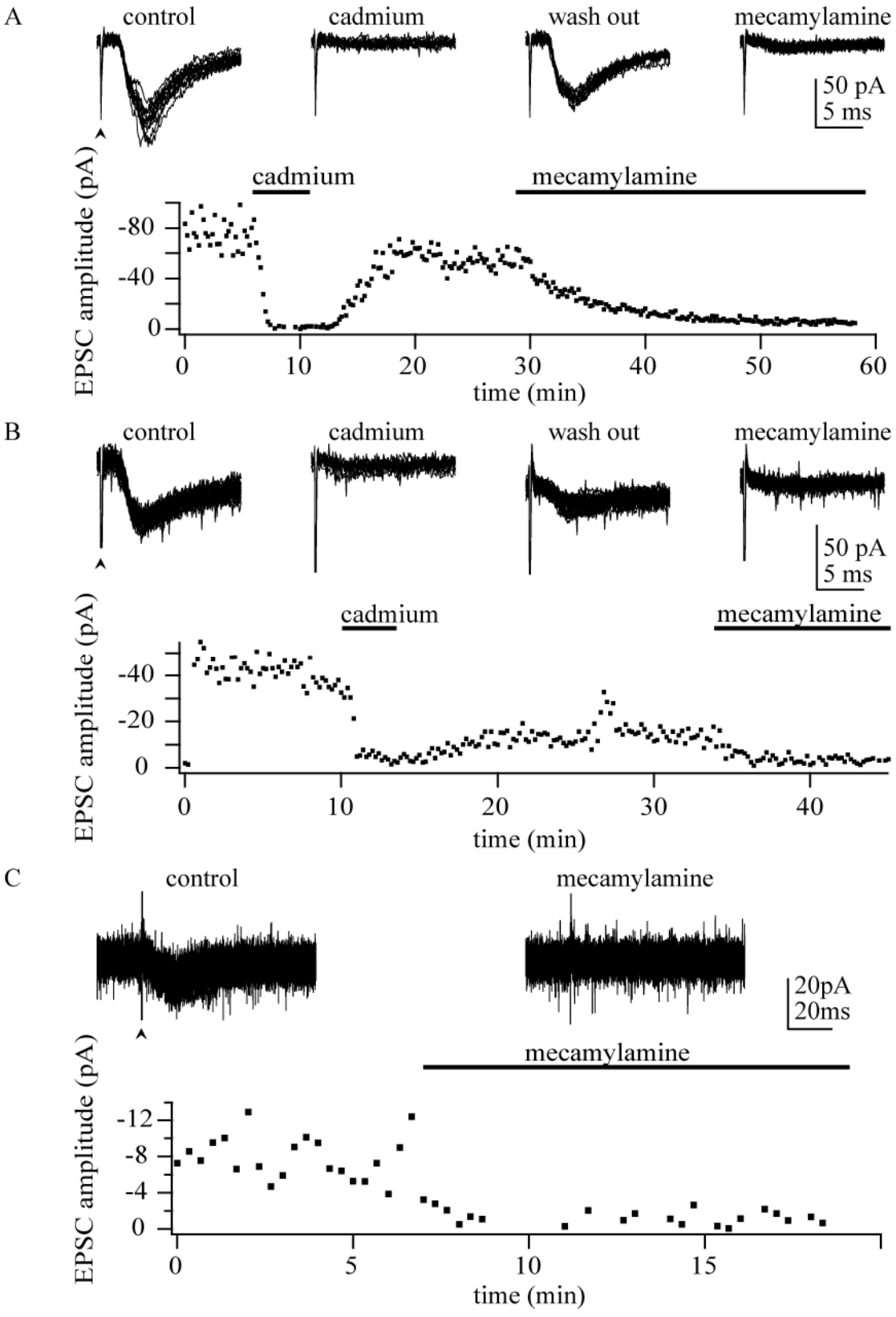

Figure 2.6: (Continued)

around this region often damaged or destroyed the labellar nerve, probably due to the fine structure of how the perineural sheath connects this region with the nerve.

Physiological taste stimulation

The promising results from the electrophysiological screen described above convinced us that it was worth the effort to work out a new preparation to record from our candidate neurons while delivering tastants to the proboscis. This task was quite difficult, given the stringent requirement of keeping the proboscis dry while recording from candidate neurons. (In pilot experiments, we found that GRNs which were constantly submerged in saline did not seem to respond to stimulation of the proboscis by pressure-ejected tastant solutions.) We also needed some way to deliver tastants to the proboscis in a reliable, timed, and repeatable fashion.

We therefore developed a method of tastant delivery using a piezoelectric actuator (Figure 2.7, also see Methods). This enabled us to simultaneously make whole-cell patch clamp recordings from our candidate gustatory neurons *in vivo* while stimulating the proboscis with different tastants. Both the piezoelectric device and the proboscis were situated on the ventral (lower) side of the platform which held the fly, and so were separated from the saline bathing the brain. This allowed us to keep the proboscis dry.

The response evoked by tastant stimulation in the candidate neuron labeled by the *c600-Gal4* was similar across all taste modalities (Figure 2.8A). Bitter, salty, sweet, and water tastants all elicited a similar response – namely, a small depolarization at the onset and offset of the stimulus that was often accompanied by a single spike. The untuned nature of this neuron's response to different classes of tastants seemed more indicative of

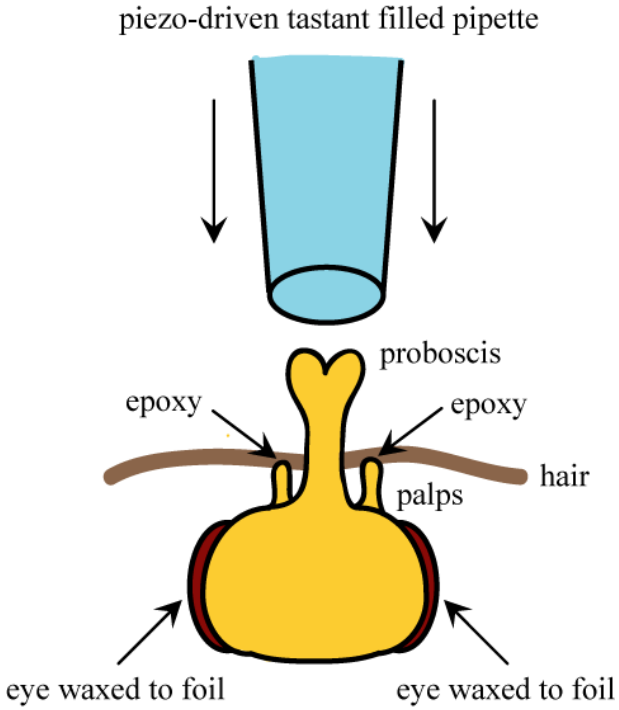

Figure 2.7: Schematic of preparation for patch clamp recordings of candidate taste neurons while delivering tastants to proboscis. This view is from the ventral side of the platform. The recording electrode is dorsal to the platform, and so not visible here. The proboscis is kept dry when not exposed to tastant stimuli.

Figure 2.8: Tastant evoked responses of candidate taste neuron cell bodies. These recordings show responses (or lack thereof) to simulation of the proboscis with tastants. *A*: untuned response of a candidate taste neuron labeled by *c600-Gal4*. Note that all classes of tastants elicit the same response, implying that it is the mechanical (rather than chemical) component of this stimulus which is causing the response. Several traces are overlaid to show trial-to-trial variability. *B*: a candidate taste neuron labeled by *a159-Gal4* fires bursts spontaneously in a manner which is independent of the taste stimulus. As a result, traces aligned according to stimulus onset do not show consistent burst timing. *C*: a candidate taste neuron labeled by *a125-Gal4* was wholly unresponsive to taste stimulation. Stimulus period in gray

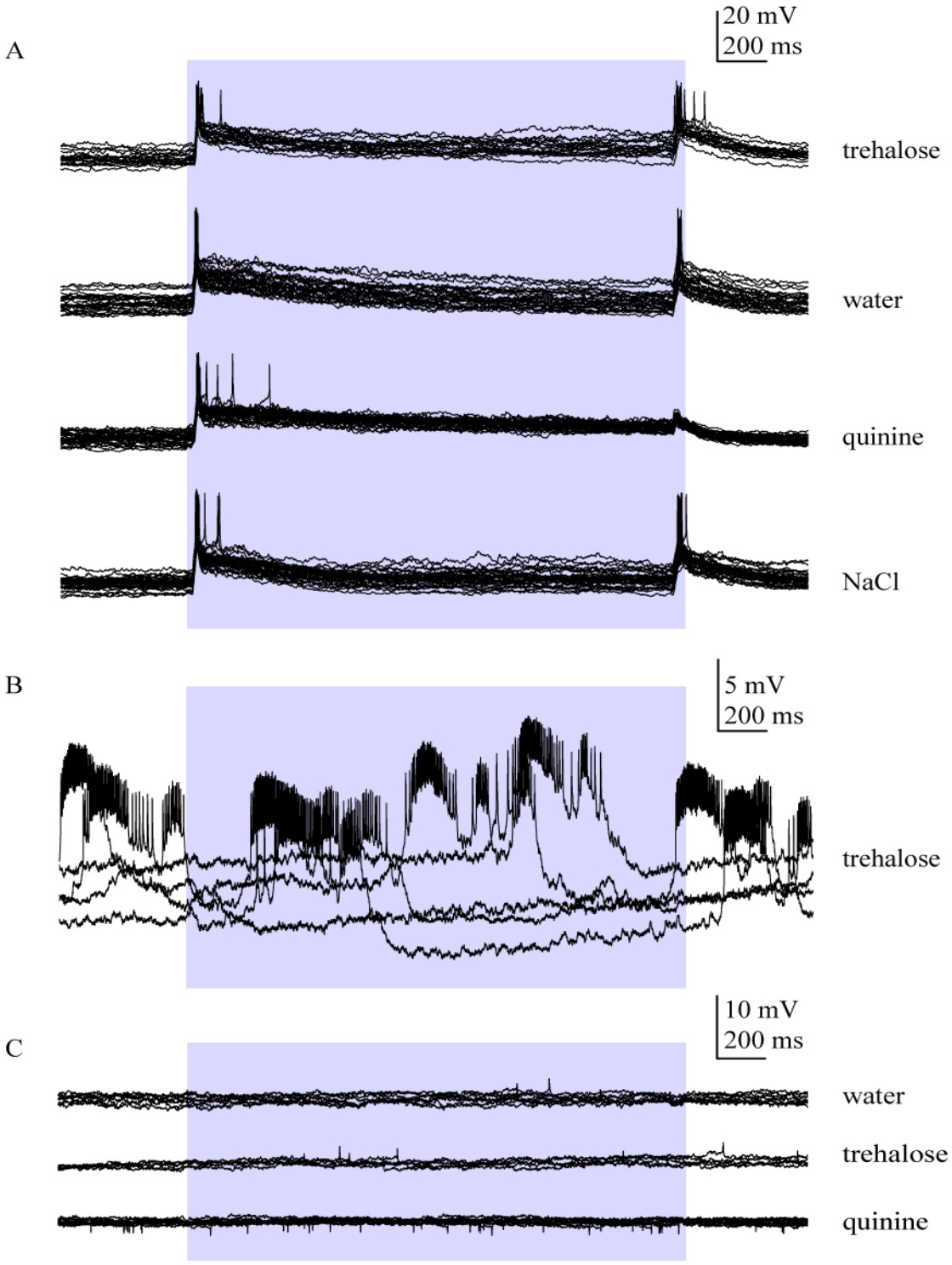

Figure 2.8: (Continued)

a mechanosensitive neuron than a taste neuron. Thus, we tentatively concluded that these neurons are probably mechanosensitive rather than gustatory.

Next, we found that the candidate neuron labeled by *a159-Gal4* seemed to burst rhythmically in a manner that was wholly independent of tastant stimulation (Figure 2.8B). Visual inspection revealed that this neuron's bursting rhythm seemed to be well correlated with the spontaneous physical movements of the proboscis. Thus, this neuron seemed to be more closely connected with the motor output of the proboscis than with gustatory processing. We tentatively concluded that these are motor neurons, or perhaps pre-motor neurons involved in a central pattern generator driving spontaneous rhythmic proboscis movements.

The candidate neuron labeled by *a125-Gal4* showed no spontaneous activity, and was wholly unresponsive to any class of tastant (Figure 2.8C). Thus, it was deemed to be unlikely involved in gustatory processing.

Finally, we found that the candidate neuron labeled by *T2-Gal4* is located in a position which was inaccessible to recording in our intact, in vivo preparation. Namely, this neuron is located on the ventral edge of the brain, immediately dorsal to the proboscis. Because of how close this neuron was to the proboscis, we were unable to record from this neuron while delivering tastants to the proboscis.

DISCUSSION

We decided to cease work on this project because we had run out of viable candidates. Based on the results of our tastant stimulation experiments (Figure 2.8), we concluded that the candidates that we had identified were not true gustatory neurons.

Rather, they appeared to represent mechanosensory neurons, motor neurons, or neurons unrelated to either sensory or motor functions of the proboscis.

Unfortunately, we were unable to make patch clamp recordings from the promising candidate labeled by *T2-Gal4* while delivering tastants to the proboscis. These neurons innervated the SOG and also sent processes through the putative output tract of the SOG. We tried for some time to adjust our preparation to enable patch clamp recordings from the candidate gustatory neurons labeled by *T2-Gal4*, but the position of these neurons was too close to the proboscis. We considered using a genetically encoded calcium indicator in lieu of electrophysiological recordings to characterize the response of these neurons, but at the time of our study, the sensitivity of these genetic indicators was too low to enable precise characterization of taste receptive fields (Pologruto, Yasuda et al. 2004).

The advantage of working in *Drosophila* neuroscience is that the existence of the Gal4/UAS enhancer trap system (Brand and Perrimon 1993) has made it possible to complete studies on specific sets of neurons. However, because of the organization of the *Drosophila* brain (where neurons innervating a particular neuropil may have cell bodies in any location), it is also difficult to complete studies in *Drosophila* neurobiology without having a good Gal4 line. Neurons adjacent to one another physically may have vastly different projection patterns, given the relative small size of *Drosophila* brain. Thus, it is not sufficient to know generally where the cell bodies of interest are located. We must have a genetic label to unambiguously identify them for study across different animals. We did in fact make whole-cell patch-clamp recordings from unlabeled neurons immediately dorsal to the anterior region of the SOG. This was the region of the fly brain

that was revealed by our calcium imaging experiments to contain a large number of cells responsive to simulation of the labellar nerve (Figure 2.3). However, we found in these blind recordings that only a small percentage (<10%) of neurons responded to nerve stimulation (data not shown). The response in these neurons was also extremely varied, making it difficult to study them systematically. Thus, because completing our proposed study would have been very difficult without a good Gal4 line and we had run out of viable candidate Gal4 lines, we decided to stop pursuing this project.

Reflecting on our general approach and strategy, there are two strategic decisions that might have been made differently, given what we now know. First, we could have perhaps placed more priority at the outset of the project on developing the preparation with *in vivo* taste stimulation of the proboscis, instead of focusing so much on electrical stimulation of the labellar nerve. This would have enabled us to generate better candidates and to have allowed us to assess viability of the different candidates much sooner than we did. We did not do this because we knew from the beginning that the *in vivo* recording would be a very laborious and difficult task, and we did not wish to invest in this task without first investigating whether there were indeed any good candidate Gal4 lines. In addition, the details of this preparation would heavily depend on the precise location of the candidate neurons, which made it seem attractive to identify our candidate neurons before developing the preparation. Thus, it did not seem to us to be a good investment of time to develop a preparation that would potentially be unusable for a large pool of potential candidate neurons.

Second, we could have also used different methods to activate GRNs. As the labellar nerve houses the axons of olfactory neurons as well as mechanosensitive neurons

in addition to that of GRNs, it is perhaps unsurprising that our nerve stimulation screen generated candidates that were unrelated to taste. We could have potentially avoided this pitfall by using a more selective way to stimulate GRNs. Specifically, we might have used genetically-encoded triggers of neuronal activity, such as the P2X2 receptor (Zemelman, Nesnas et al. 2003) or channelrhodopsin (Boyden, Zhang et al. 2005) to selectively activate GRNs. However, there is no single Gal4 driver that labels the majority of GRNs; rather, all known Gal4 drivers are restricted to specific classes of GRNs. Thus, we would have had to increase the number of screens we completed commensurate with the number of classes of gustatory receptors we wanted to test. The labellar nerve also contained a nice internal positive control in housing the axons of olfactory receptor neurons of the maxillary palps. There would have been no simple, within-preparation positive control for the efficacy of our stimulus had we taken these alternate approaches. Our thinking in taking the approach we did was to err on the side of generating too many rather too few candidates.

We were ultimately unsuccessful in identifying and characterizing central gustatory neurons in *Drosophila*. However, we believe that this failure was due to a lack of specific Gal4 lines rather than our general approach. This, in turn, reflects the relative poverty of Gal4 lines that are publicly available at this time. In the future, if more lines become publicly available, particularly if images of these innervation patterns of these lines are also available, then a strategy like this would be likely to generate many more useful candidates. We believe that our strategy of using the combination of calcium imaging and PA-GFP to identify groups of neurons functionally and anatomically

connected to peripheral sensory neurons is generally applicable toward generating good candidate central neurons associated with other sensory modalities.

REFERENCES

Boyden, E. S., F. Zhang, et al. (2005). "Millisecond-timescale, genetically targeted optical control of neural activity." Nat Neurosci **8**(9): 1263-1268.

Brand, A. H. and N. Perrimon (1993). "Targeted gene expression as a means of altering cell fates and generating dominant phenotypes." Development **118**(2): 401-415.

Carter, A. G. and B. L. Sabatini (2004). "State-dependent calcium signaling in dendritic spines of striatal medium spiny neurons." Neuron **44**(3): 483-493.

Clyne, P. J., C. G. Warr, et al. (2000). "Candidate taste receptors in Drosophila." Science **287**(5459): 1830-1834.

Datta, S. R., M. L. Vasconcelos, et al. (2008). "The Drosophila pheromone cVA activates a sexually dimorphic neural circuit." Nature **452**(7186): 473-477.

Dunipace, L., S. Meister, et al. (2001). "Spatially restricted expression of candidate taste receptors in the Drosophila gustatory system." Current Biology **11**(11): 822-835.

Falk, R., N. Bleiser-Avivi, et al. (1976). "Labellar taste organs of Drosophila melanogaster." Journal of Morphology **150**(2): 327-341.

Fiala, A., T. Spall, et al. (2002). "Genetically expressed cameleon in Drosophila melanogaster is used to visualize olfactory information in projection neurons." Current Biology **12**(21): 1877-1884.

Gordon, M. D. and K. Scott (2009). "Motor control in a Drosophila taste circuit." Neuron **61**(3): 373-384.

Hiroi, M., F. Marion-Poll, et al. (2002). "Differentiated response to sugars among labellar chemosensilla in Drosophila." Zoological Science **19**(9): 1009-1018.

Hiroi, M., N. Meunier, et al. (2004). "Two antagonistic gustatory receptor neurons responding to sweet-salty and bitter taste in Drosophila." J Neurobiol **61**(3): 333-342.

Horowitz, L. F., J. P. Montmayeur, et al. (1999). "A genetic approach to trace neural circuits." Proc Natl Acad Sci U S A **96**(6): 3194-3199.

Morante, J. and C. Desplan (2004). "Building a projection map for photoreceptor neurons in the Drosophila optic lobes." Semin Cell Dev Biol **15**(1): 137-143.

Nakai, J., M. Ohkura, et al. (2001). "A high signal-to-noise Ca(2+) probe composed of a single green fluorescent protein." Nature Biotechnology **19**(2): 137-141.

Ng, M., R. D. Roorda, et al. (2002). "Transmission of olfactory information between three populations of neurons in the antennal lobe of the fly." Neuron **36**(3): 463-474.

Olsen, S. R., V. Bhandawat, et al. (2007). "Excitatory interactions between olfactory processing channels in the Drosophila antennal lobe." Neuron **54**(1): 89-103.

Patterson, G. H. and J. Lippincott-Schwartz (2002). "A photoactivatable GFP for selective photolabeling of proteins and cells." Science **297**(5588): 1873-1877.

Pologruto, T. A., B. L. Sabatini, et al. (2003). "ScanImage: flexible software for operating laser scanning microscopes." Biomed Eng Online **2**: 13.

Pologruto, T. A., R. Yasuda, et al. (2004). "Monitoring neural activity and [Ca2+] with genetically encoded Ca2+ indicators." J. Neurosci. **24**(43): 9572-9579.

Rajashekhar, K. P. and R. N. Singh (1994). "Neuroarchitecture of the tritocerebrum of Drosophila melanogaster." J Comp Neurol **349**(4): 633-645.

Scott, K., R. Brady, Jr., et al. (2001). "A chemosensory gene family encoding candidate gustatory and olfactory receptors in Drosophila." Cell **104**(5): 661-673.

Shanbhag, S. and R. N. Singh (1992). "Functional implications of the projections of neurons from individual labellar sensillum of Drosophila melanogaster as revealed by neuronal-marker horseradish peroxidase." Cell and Tissue Research **267**: 273-282.

Stocker, R. F. (1994). "The organization of the chemosensory system in Drosophila melanogaster: a review." Cell and Tissue Research **275**(1): 3-26.

Thorne, N., C. Chromey, et al. (2004). "Taste perception and coding in Drosophila." Current Biology **14**(12): 1065-1079.

Wang, J. W., A. M. Wong, et al. (2003). "Two-photon calcium imaging reveals an odor-evoked map of activity in the fly brain." Cell **112**(2): 271-282.

Wang, Z., A. Singhvi, et al. (2004). "Taste representations in the Drosophila brain." Cell **117**(7): 981-991.

Wickersham, I. R., D. C. Lyon, et al. (2007). "Monosynaptic restriction of transsynaptic tracing from single, genetically targeted neurons." Neuron **53**(5): 639-647.

Wilson, R. I. and G. Laurent (2005). "Role of GABAergic inhibition in shaping odor-evoked spatiotemporal patterns in the Drosophila antennal lobe." J. Neurosci. **25**(40): 9069-9079.

Wilson, R. I., G. C. Turner, et al. (2004). "Transformation of olfactory representations in the Drosophila antennal lobe." Science **303**(5656): 366-370.

Yasuyama, K. and P. M. Salvaterra (1999). "Localization of choline acetyltransferase-expressing neurons in Drosophila nervous system." Microsc Res Tech **45**(2): 65-79.

Zemelman, B. V., N. Nesnas, et al. (2003). "Photochemical gating of heterologous ion channels: remote control over genetically designated populations of neurons." Proceedings of the National Academy of Sciences of the United States of America **100**(3): 1352-1357.

CHAPTER 3:

Transduction in *Drosophila* olfactory receptor neurons is invariant to air speed

INTRODUCTION

For all terrestrial animals, the sense of smell is directly connected to the movement of air. Terrestrial vertebrates draw air into their nose using active sniffing behaviors, and air speed within the nose has been shown to be a critical variable in determining the magnitude of odor responses in olfactory receptor neurons (ORNs). Specifically, ORN response magnitudes tend to increase with increasing air speed, given a fixed odor concentration and odor pulse duration (Doving 1987; Mozell et al. 1991a; Mozell et al. 1991b; Scott et al. 2006; Sobel and Tank 1993). Accordingly, the perceived odor intensity of a fixed odor concentration in humans can grow with increasing air speed through the nose (Le Magnen 1944; Rehn 1978; Schneider et al. 1963). Olfactory performance in both humans and rodents can depend on sniff rate (Kepecs et al. 2007; Laing 1983), a phenomenon that may be mediated by the effect of air speed on ORN responses.

What are the reasons why air speed might affect olfactory transduction? Four explanations have been proposed on the basis of previous studies (Figure 3.1):

A. Mechanosensitivity: ORNs may be intrinsically responsive to mechanical stimuli. In particular, odorant receptor proteins have been proposed to be force-activated as well as ligand-activated. This conclusion was suggested by the finding that the responses of mouse ORNs *in vitro* can grow with increasing delivery pressure of Ringer's solution (Grosmaitre et al. 2007). Given this, increasing air speed might be expected to increase ORN responses.

Figure 3.1: Proposed mechanisms of air speed dependence in olfactory transduction. Arrows indicate the direction of the air movement, and the density of black dots indicates relative odor concentration. *A*: increases in air speed can exert forces on olfactory receptor neurons (ORNs), thereby leading to displacements that activate intrinsically mechanosensitive conductances in ORNs. Note that this is the only mechanism that does not invoke a spatial non-uniformity in odor concentration. *B*: a boundary layer of air can form around the olfactory organ where odor concentration is lower than the concentration outside this layer. Because the layer should become thinner with increasing air speed, its effect is diminished as air speed increases. *C*: the olfactory organ might act as a sieve which captures odor molecules. If capture were essentially irreversible, then the rate of capture (and thus local odor concentration) would grow with increasing air speed. *D*: in the vertebrate nasal cavity, odorized air is drawn over a large absorptive surface which can progressively deplete odor from the air, forming a gradient of odor concentration through the length of the cavity. The steepness of the gradient should decrease with increasing air speed, and so increasing air speed should increase the odor concentrations that are delivered to downwind sites in the cavity. For ORNs which are located downwind, this would increase odor responses.

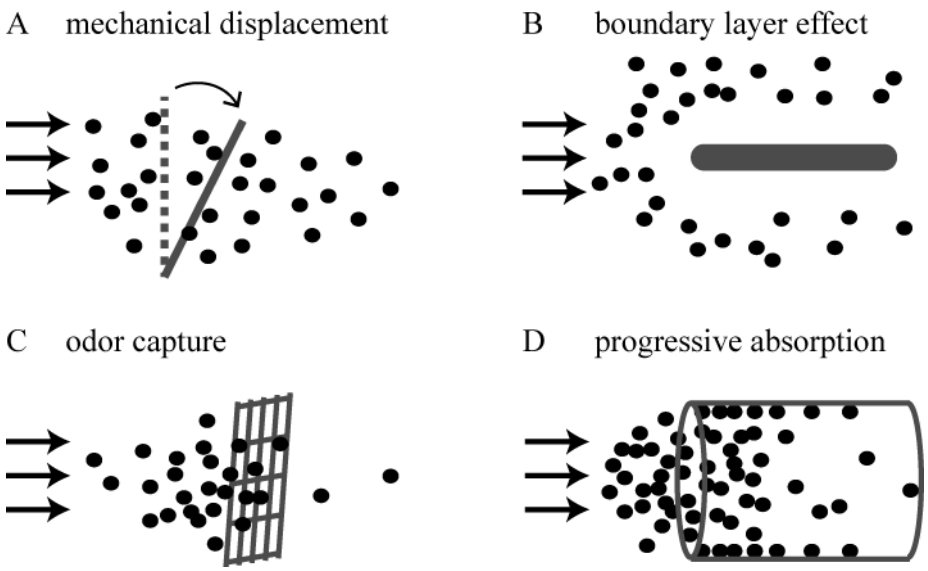

Figure 3.1: (Continued)

B. Boundary layer thinning: At low air speeds, an object will be surrounded by a layer of slow-moving air (the "boundary layer") (Koehl 2006; Moore et al. 1989). This boundary layer slows the movement of odor molecules to the olfactory organ, lowering the effective concentration of odor at the receptors. Increasing air speed decreases the thickness of the boundary layer. This creates better penetration of odor molecules into the surface of the olfactory organ – e.g., into crevices of the nasal cavity (Mozell et al. 1991b), or gaps between hairs on the surface of insect antennae. Similarly, at high water flow rates, aqueous odor penetrates more deeply between hairs on crustacean antennules (Koehl 2006). As a result, increasing air speed can increase odor concentration at the surface of the olfactory organ.

C. Increased odor capture: This model treats the olfactory organ as a molecular "sieve" which captures much of the odor in its vicinity and makes the odor available to ORNs (Kaissling 1971; Kaissling 1986). The rate of odor delivery into the sieve will be proportional to air speed. If the probability of an incoming odor molecule being captured by the sieve is independent of air speed, then the local odor concentration will increase with air speed. For this to be true, it is also important that the rate of removal of odor from the sieve does not keep pace with the increasing rate of odor delivery. Evidence for this model comes from measurements showing that about a third of radioactive pheromone molecules passing over a moth antenna are absorbed and not readily released (Kanaujia and Kaissling 1985). The finding that some ORN responses far outlast the duration of the nominal stimulus has been cited as further evidence that captured odor is not readily removed

(Kaissling 1971). How this process might work on a microscopic level is not known.

D. Decreased pre-absorption: In the vertebrate nose, odor enters at the nostrils and moves through the long, closed path of the nasal cavity. At each location in this path, some odor is absorbed into the mucosa, and some of this absorbed odor may be actively removed (e.g., by diffusing into capillaries) rather than returning to the air. This effect can create a gradient of odor concentration along the nasal cavity, with lower concentrations at locations more distal to the nostrils. If increasing air speed decreases the probability of an odor molecule being absorbed at any location in the path (because its dwell time at that location decreases), then increasing air speed will make the gradient more shallow. This means that distal ORNs will be exposed to higher odor concentrations. This effect should be largest for odors that are most readily absorbed into mucous – i.e., hydrophilic odors (Kent et al. 1996; Mozell and Jagodowicz 1973; Mozell et al. 1991a; Mozell et al. 1991b; Schoenfeld and Cleland 2005; Scott et al. 2006).

In thinking about the effects of air speed on olfaction, it is worth thinking about whether the organism actively controls air speed. Whereas vertebrates control the flow of air through their nose, many insects have comparatively little control over air flow across their olfactory organs. Much of the air movement across insect olfactory organs is driven by wind in the environment, although wing and antennal movements can play a role (Dethier 1987; Loudon and Koehl 2000; Mamiya et al. 2011). Because insects cannot fully control this stimulus parameter, it is important to understand whether it might confound insect olfactory transduction.

Three of the mechanisms described above (A, B, and C) might plausibly apply to insect olfactory organs. (The fourth mechanism would not apply, because unlike air moving through the vertebrate nasal cavity, air moving across an insect antenna is not confined to a long, closed path.) No previous studies have directly measured whether air speed affects olfactory transduction in insects. Nevertheless, many theoretical studies and review articles have proposed or assumed that olfactory transduction in insects grows with increasing air speed (Kaissling 1971; Kaissling 1986; 1998; 2001; Kaissling and Rospars 2004; Lansky and Rospars 1998; Rospars et al. 2000).

It is of particular interest to know whether olfactory transduction in *Drosophila* depends on air speed because of the general interest in exploiting the genetic toolbox of *Drosophila* to study olfactory transduction, processing, and learning (Davis 2011; Hallem and Carlson 2004; Masse et al. 2009; Olsen and Wilson 2008; Ramdya and Benton 2010). Like most insect ORNs, *Drosophila* ORNs are housed in hair-like structures (called sensilla) on the surface of the antenna (Keil 1999). By inserting a fine electrode into a single sensillum, one can record from individual ORNs *in vivo* (de Bruyne et al. 1999; de Bruyne et al. 2001). An experimental virtue of this preparation is the ability to unambiguously identify different ORN types in these recordings, where a "type" is defined by the odorant receptor that an ORN expresses (Couto et al. 2005; Fishilevich and Vosshall 2005).

In this study, we constructed and validated an odor delivery device designed to independently control odor concentration and air speed. We used this device to test whether air speed affects olfactory transduction in two different types of *Drosophila* ORNs *in vivo*. Given that the dependence of transduction on air speed has been proposed

to be related to the hydrophobicity of the odor, we used three different odors with widely varying hydrophobicity. Our results argue that olfactory transduction in *Drosophila* is invariant to air speed, at least within the parameter space we have explored. This has implications for the mechanisms of odor delivery from the perireceptor space in *Drosophila* ORNs. It also implies that an organism that cannot fully control air flow over its olfactory organ is capable of evolving air speed-invariant mechanisms of olfactory transduction. This stands in contrast to vertebrate olfactory systems, where air speed is both critical to transduction and under the control of the organism.

METHODS

Odor delivery

We designed a custom odor delivery device to allow independent control over air speed and odor concentration (Figure 3.2A). A continuous stream of charcoal-filtered air was fed into two adjustable flow meters set to the same flow rate. Depending on the range of air speeds that was desired in the experiment, we used a different pair of matched flow meters (127657-1, 234509-1, or 277577-1 from Cole-Parmer), permitting maximum flow rates of 300 mL/min, 2.5 L/min, or 10 L/min (indicated in black, light gray, and dark gray in Figure 3.3B). By controlling the flow rate through these flow meters, we could control the speed of the final odorized air stream. The output of one of the two flow meters was sent to a large bubbler (7538-29, Ace Glass) where air was forced through a glass diffuser and up through a large column of pure liquid odorant to produce saturated (or nearly-saturated) vapor in the head space of the bubbler. This odorized air stream and the matched clean air stream were each delivered to a three-way

Teflon solenoid valve (STV-3-1/4 UKG 24VDC, Clark Solutions). These two valves were controlled via a microcontroller platform (Arduino Nano, Arduino Software) and custom routines written in MATLAB. The two valves were always held in opposite states, such that at any moment one line would be vented, while the other line would be passed to an odor/air mixing chamber. The two valves were programmed to alternate between the vent and the mixing chamber with a period of one second. By varying the duty cycle of this switching, we could vary the ratio of odorized air to clean air that was delivered to the mixing chamber and thus the equilibrium odor concentration in the mixing chamber. The mixing chamber was a 500-mL glass Erlenmeyer flask. We allowed five minutes to elapse after any change in the duty cycle to permit the odor concentration in the flask to re-equilibrate before odor was delivered to the fly. The output of the mixing flask was delivered to a third and final solenoid valve that could be switched between a vent and the fly. This last valve allowed us to control the duration of the odor pulse. All odor stimuli were 5 sec in duration and are reported as nominal percentages of saturated vapor. All the odor vents in the system were positioned near a vacuum tube, but were not connected to this tube, and thus there was essentially no negative pressure on the vents. The final odor tube had an inner diameter of 3 mm and terminated less than 1 mm away from the fly (Figure 3.2B). The water solubility values for dibutyl sebacate and 1-propanol are taken from (Yalkowsky et al. 2010), and the water solubility of linalool oxide was estimated using the U.S. Environmental Protection Agency's EPI Suite software (v. 4.10).

Note that the odor pulse duration was constant for all air speeds, meaning that the total number of delivered odor molecules per odor pulse grew proportionately with

increasing air speed. Some authors have pointed out that it can be useful to keep the number of delivered molecules constant (Mozell et al. 1991b), especially when olfactory transduction depends on air speed. However, when transduction depends only on odor concentration (as it does in our results), keeping odor pulse duration constant does not introduce any confounds in interpretation.

We noticed that as air speeds increased above 5 m/s, the measured odor concentration at the outlet of the device showed a small systematic decrease (≤ 10% of maximum; Figure 3.3). This is likely due to the fact that high flow rates cause high pressures in the system, which can cause odor vapor to leak out prior to mixing. This effect was often statistically significant: when we ran separate linear regressions of measured odor concentration versus air speed for each combination of odor and duty cycle, we often noted a statistically significant negative linear correlation between these values. This likely explains why we noticed a non-significant trend toward decreased ORN firing rates with increasing air speeds for certain odor and duty cycle settings. This phenomenon did not appear to significantly influence our ORN recordings (see below), probably because it is relatively small in magnitude.

Photoionization and anemometer measurements

We used a photoionization detector (PID; 200A miniPID, Aurora Scientific Inc.) to measure the magnitude and time course of the odor pulse at the output of the last valve. The magnitude of the PID signal is proportional to odor concentration, with the proportionality constant depending on the odor composition. The PID is capable of reporting concentration fluctuations at speeds of up to 330 Hz, according to the

manufacturer. The PID inlet was positioned 1 mm from the fly, downwind from the valve, and was used to measure the output of the device for all experiments using air speeds >1 m/s (Figure 3.2B). The PID was operated on the low flow rate setting (970 mL/min), and we verified that ORN responses were the same regardless of whether the PID was turned on or off, for all experimental conditions where the PID was used (i.e., for air speeds >1 m/s). The glass bulb inside the PID head was cleaned periodically to remove accumulated residue which diminished PID sensitivity. In spite of this, the PID sensitivity drifted slowly over the time course of days, and therefore PID values were normalized to a within-experiment measurement before they were averaged across experiments (see Data analysis). The accuracy of the PID was diminished at flow rates below 2.0 L/min (corresponding to 2.67 m/s at the outlet of our final valve) because the negative pressure exerted by the PID pump was not fully balanced by the positive pressure provided by the air stream. For this reason, we did not measure PID values for the lowest range of flow rates / air speeds in our study. We measured PID responses for two of the three odors we used in this study (linalool oxide and 1-propanol), but not for the third odor (dibutyl sebacate), because it did not elicit a measureable PID signal. In order to measure air speed, we used a hot wire anemometer (Anemomaster A004, Kanomax) positioned at the location of the fly. According to the manufacturer's specifications, the anemometer does not provide accurate readings below 0.1 m/s, and therefore the reading of 0.06 m/s (Figure 3.8B) should be regarded with caution. We were not able to obtain stable readings below 0.06 m/s, and so we did not investigate air speeds below this value in this study. In addition, at air speeds lower than this value, odor delivery tends to become turbulent.

Electrophysiology

Flies were reared at room temperature on conventional cornmeal agar medium. All ORN recordings were performed on adult female flies from the wild-type strain w^{1118}, 2-5 days after they eclosed from their pupal cases. Flies were cold-anesthetized and wedged into the trimmed end of a 200-microliter plastic pipette tip. Each fly was secured by waxing the head and proboscis to the end of the pipette tip. The fly was then placed under an upright compound microscope (Olympus BX51) with a 50× air objective. A video camera pointed at the head of the fly (Unibrain Fire-I BBW 1.3 Camera, equipped with an 8mm telephoto lens, 1394Store.com) allowed the fly to be positioned precisely relative to the odor tube and the PID. The antenna was stabilized using two pulled glass capillaries fashioned with small hooks at the ends. The recording and reference electrodes were silver chloride wires inserted into saline-filled glass electrodes. The recording electrode was inserted into a single antennal sensillum while the reference electrode was inserted into the eye (Figure 3.2B). Sensillum types were identified based on their size, the spike waveforms and spontaneous firing rates of the neurons in the sensillum, and the responses of the neurons to a panel of odors (de Bruyne et al. 2001). Voltage signals were acquired with an A-M Systems Model 2400 amplifier and low-pass filtered at 2kHz with a LPF202A signal conditioner (Warner Instruments) before digitization at 10 kHz. Digitized signals were acquired using custom routines written in IgorPro (Wavemetrics) through a PCI-6251 data acquisition board (National Instruments). The sample trace shown in Figure 3.5A was high-pass filtered at 15 Hz post-digitization to remove the slow local field potential component of the response.

Data analysis

Spikes were identified using custom routines written in IgorPro (Wavemetrics) that filtered, differentiated, and thresholded the raw signal. Statistics were computed in MATLAB (Mathworks). Except in Figure 3.4 and in Figure 3.9, all firing rates and PID measurements were averaged over the entire five-second duration of the odor pulse. In Figures 3.3A and 3.3B, each PID value was normalized to the value measured in that experiment at an air speed of 4.0 m/second at the highest duty cycle, and then averaged across all trials and experiments. This corrects for the fact that the absolute sensitivity of the PID can drift slowly on a time scale of days. In Figures 3.5-3.8, firing rates were first averaged across three trials using the same stimulus in the same experiment; these values were then averaged across experiments, and the figures report the mean ± SEM across experiments. Peri-stimulus time histograms in Figure 3.5B and Figure 3.9 were calculated by accumulating spikes across trials within an experiment, convolving spike times with a Hanning window (200 ms for Figure 3.5B, 50 ms for Figure 3.9), and then averaging the resulting histogram across experiments. In Figure 3.9, each histogram was normalized to its maximum value before averaging across experiments, in order to allow comparison of response dynamics across different air speeds.

In order to assess whether firing rate exhibited any statistically significant dependence on either concentration or air speed, we performed a three-step statistical procedure. First, we performed a repeated-measures two-way ANOVA test corresponding to each condition (where a "condition" is defined as specific neuron, odor, and set of flow meters). In other words, we performed a separate ANOVA test for each of the panels in Figures 3.5C, 3.5D, 3.6, 3.7A, 3.7B, 3.8A, and 3.8B. Second, in the event

that we observed a significant effect of air speed for a given condition, we then performed post hoc paired *t*-tests for all possible pair-wise comparisons between air speeds for each odor concentration tested under that condition. For example, for ab2A and linalool oxide (panel in Figure 3.5C), we performed a total of 30 pair-wise comparisons (10 comparisons each for 10%, 25%, and 50%). The results of each of these tests were subjected to a Bonferroni correction, and the *p* values reported in the text reflect this correction. Third, in the event that any of these corrected values indicated a significant difference between the firing rates measured at different air speeds, we then asked whether there was a statistically significant linear correlation between measured odor concentration (i.e., PID voltage) and air speed for that particular set of experiments. If so, then this would be evidence that we had failed to actually keep concentration constant in these experiments.

RESULTS

Independent control of air speed and odor concentration

To assess whether olfactory transduction in *Drosophila* is dependent on air speed, we needed to be able to control odor concentration independent of the air speed (and thus flow rate) through the device. This is difficult to achieve in a conventional odor delivery device for two reasons. First, a device with a limited head space of odor vapor is depleted at a rate that depends on the rate of flow through the system. As a result of this, changing

Figure 3.2: Experimental setup. *A:* schematic of the odor delivery device. Air speed was controlled by changing the flow through two matched flow meters which were set to the same flow rate. The output of one flow meter was sent through a large column of pure liquid odorant, producing saturated (or nearly-saturated) vapor. The odorized air stream and its matched clean air stream were each sent to a three-way valve. These two valves were always held in opposite states so that only one would be passed to the mixing chamber at any given time while the other was vented. The concentration of the final odor pulse was controlled by altering the duty cycle of switching between the valves. The timing of the final odor pulse was controlled by a valve near the fly. *B:* scale diagram of the recording configuration, as seen from above, through the microscope objective. The fly was placed in as close as possible to odor tube and the photoionization detector (PID). A miniature video camera near the fly's head permitted precise positioning of the fly. One antenna was lifted off the fly's head and stabilized using a pair of fine glass hooks. The recording electrode was inserted into a sensillum on this antenna, and the ground electrode was inserted into an eye.

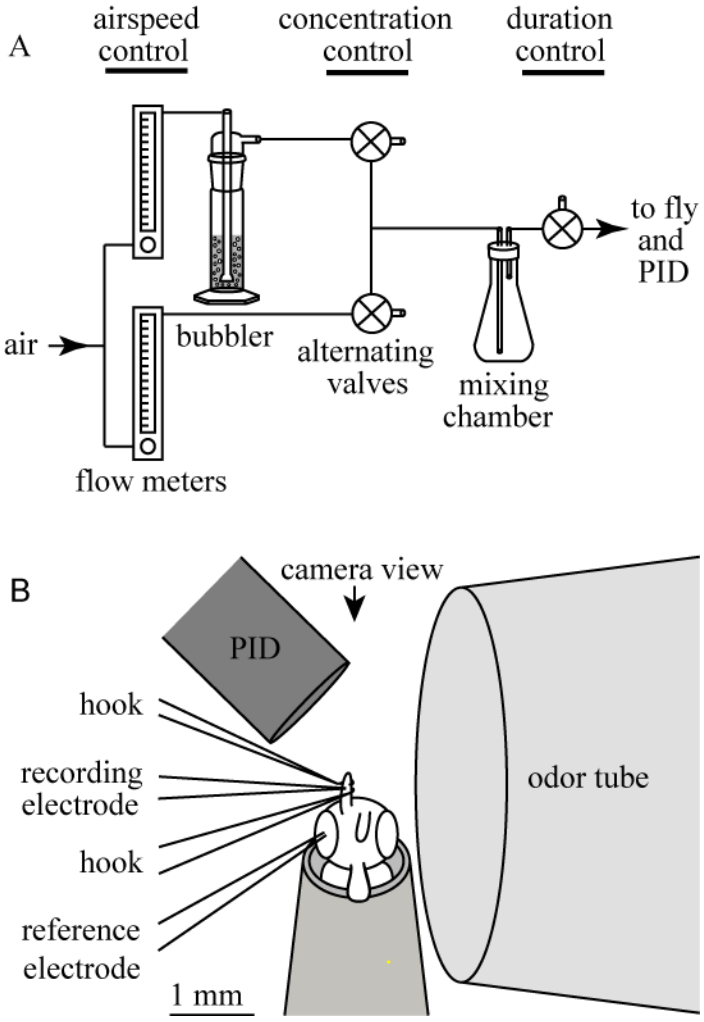

Figure 3.2: (Continued)

the flow rate will also tend to change odor concentration. Second, most conventional devices vary odor concentration by diluting odor in quasi-odorless liquid solvent, such as paraffin oil. However, many solute-solvent pairs deviate from ideal solution assumptions (Raoult's law), and thus yield vapor mixtures where the ratio of solute to solvent differs from the ratio in the liquid phase. For example, if the ratio of odor to solvent is higher in the vapor phase than in the liquid phase, then as vapor is removed from the head space, the odor will be progressively removed from the container more quickly than the solvent is removed. As a consequence, odor concentration will run down over time at a rate that increases with increasing flow rate. Both these problems can be solved by using a large head space in the container of odor and by varying odor concentration via vapor-phase dilutions rather than liquid dilutions.

For these reasons, we designed and constructed an air dilution odor delivery device with a large head space (Figure 3.2A, also see *Methods*). All measurements were taken as close as possible to the final outlet of the device (Figure 3.2B). We varied the nominal odor concentration from 0% to 50% saturated vapor, and verified that this produces a linear increase in the odor concentration at the output of the device, as measured by a photoionization detector (PID; Figure 3.3A). We also varied the flow rate through the system from 0.1 to 5.0 L/min, and verified that this produces a linear increase in the air speed at the output of the device, as measured by an anemometer (Figure 3.3B).

Importantly, this device allowed independent control of air speed and concentration. Over the range of air speeds over which the PID can operate, we confirmed that changing the air speed causes only small variations in measured odor concentration (Figs. 3C-D). The small variations are attributable to two phenomena. The

Figure 3.3: Validation of odor delivery device using photoionization detector (PID) measurements. *A:* the normalized PID voltage (which should be proportional to odor concentration at the device outlet) depended nearly linearly on the duty cycle of valve switching (which should be proportional to the concentration in the mixing chamber, reported here as percentage of saturated vapor). Data averaged over 11 experiments using linalool oxide at an air speed of 5.3m/s. *B*: airspeed (as measured by the anemometer) depended linearly on the nominal flow rates delivered through the device. Note log-log axes. This figure includes data collected with three different sets of matched flow meters, labeled here in different shades of gray (see Methods). *C:* concentration of linalool oxide delivered to the PID was independent of air speed (mean ± SEM, n = 11; some error bars are obscured by markers). *D:* concentration of 1-propanol delivered to the PID was independent of air speed (mean ± SEM; n = 20). *E:* fall-off in PID signals at low air speeds is more pronounced when the PID pump speed is high (i.e., when the PID is exerting a large negative pressure). This implies that the fall-off is an artifact of the fact that when the PID pump is not completely matched by the odor delivery device outflow, the PID will draw in clean air.

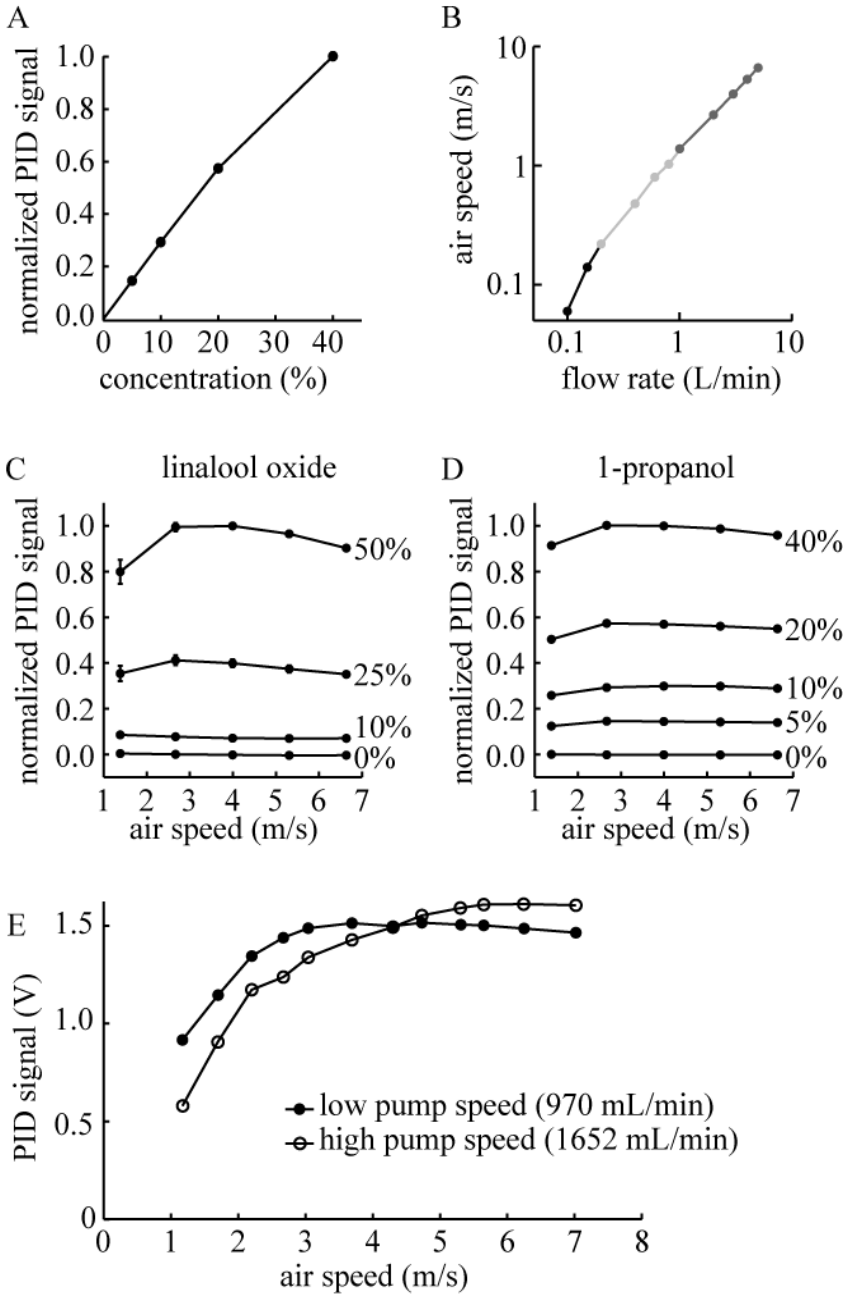

Figure 3.3: (Continued)

first phenomenon is that, at high air speeds (>5 m/s), the measured concentration showed a small systematic decrease (up to 10% of maximum) which is likely due to odor vapor leaking out of the system prior to mixing. The magnitude of this phenomenon was small, and it did not appear to influence most of our recordings, except in a few cases (see below).

A second phenomenon is that, at low air speeds (<2 m/s), the measured PID values also fall off. This is likely due to an artifact of the way the PID samples air. Namely, when the negative flow rate exerted by the PID is faster than the positive flow rate of the odor delivery device, the PID draws in clean air in addition to the odorized air, and this produces an artifactual drop in the measured concentration. Consistent with this, the threshold air speed for this fall-off depends on negative flow rate of the PID, with high negative flows producing steeper fall-off (Figure 3.3E). Because this phenomenon is an artifact, it does not indicate a true fall off in the odor concentration delivered to the fly, and as expected it did not significantly affect our ORN recordings (see below).

We also verified that the odor pulse produced by this device shows low trial-to-trial variability in its magnitude and dynamics (Figure 3.4A). This implies that the composition of the mixing chamber is constant across trials. In addition, the dynamics of the odor pulse are similar across air speeds (Figure 3.4B) and odor concentrations (Figure 3.4C).

Effect of air speed on olfactory receptor neuron responses

We delivered odor pulses of varying concentration and air speed to the *Drosophila* antenna while we made extracellular recordings of spikes from ORNs. In

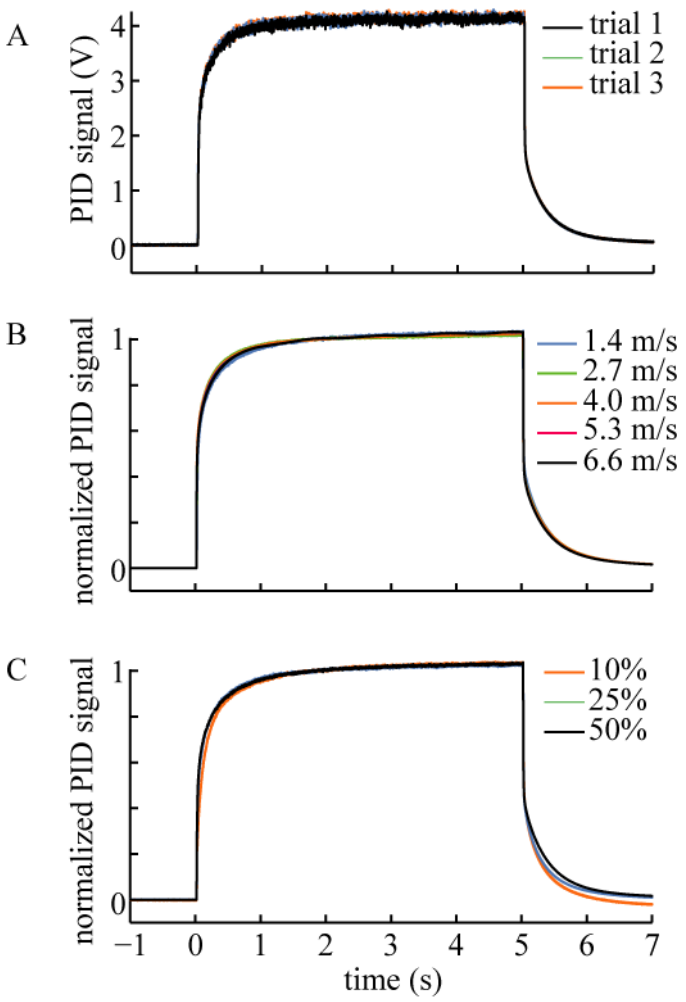

Figure 3.4: Consistency of the odor pulse delivered to the PID. *A:* consistent raw PID voltages elicited by three successive stimulus presentations (10% linalool oxide at an air speed of 2.7 m/s). *B*: consistent dynamics of normalized PID responses to the same odor at different air speeds (10% linalool oxide; n=11). *C:* consistent dynamics of normalized PID responses to the same odor at different concentrations (linalool oxide at an air speed of 2.7 m/s, n=11). Traces in *B* and *C* were normalized to their maximum value and then averaged across all trials and experiments. Note that ORN firing rates in Figures 3.5 – 3.8 were measured over the time window from 0 to 5 s.

order to probe the generality of our results, we made recordings from two different ORN types, ab2A and ab3A (de Bruyne et al., 2011). The ab2A ORN expresses the odorant receptor Or59b, and the ab3A ORN expresses the odorant receptors Or22a/22b (Hallem et al. 2004; Couto et al. 2005). We selected these ORNs because they are among the easiest to record from, and their spike waveforms are easily identifiable (Figure 3.5A, also see *Methods*).

In vertebrates, the degree to which ORN responses depend on air speed can vary with odor hydrophobicity (Kent et al. 1996; Mozell et al. 1991a; Mozell et al. 1991b; Schoenfeld and Cleland 2005; Scott et al. 2006). Also, the evidence for odor capture by insect antennae (which could in theory produce air speed dependence) derives from experiments that use extremely hydrophobic odors (Kaissling 1971; Kaissling 1986; Kanaujia and Kaissling 1985). In this study, we therefore used three different odors which collectively span a wide range of hydrophobicity values. We also deliberately used odors that produced only moderate (sub-maximal) ORN responses, in order to avoid saturating transduction.

We selected linalool oxide as our first odor because it has moderate hydrophobicity (water solubility 1.0×10^{-2} mol/L), it evokes a measureable signal in the PID, and drives moderate excitatory responses in both ORN types we recorded from (ab3A and ab2A). Increasing the concentration of this odor increased the evoked firing rate of both ORN types (Figure 3.5A-D). However, increasing the air speed (from 1.4 m/s to 6.7 m/s) had no substantial effect on firing rate (Figure 3.5A-D). Changing air speed over this range also had little effect on the dynamics of the ORN response (Figure 3.5A-B).

Figure 3.5: ORN responses to linalool oxide depend on concentration but not air speed. *A:* sample raw single-sensillum recording (top) showing the responses of the ab2A neuron to 10% linalool oxide at an air speed of 1.39 m/s. In the raw trace, the ab2A neuron corresponds to the large spike waveform (de Bruyne et al. 2001). Rasters (below) show spiking responses at different concentrations and air speeds, with three trials per condition. These representative examples show that firing rate increases with odor concentration, but is not affected by air speed. Odor pulse duration is in gray. *B*: average ORN firing rates (±SEM) plotted over time for a low and high air speed condition (50% linalool oxide, n = 7). *C*: average ab2A firing rates evoked by linalool oxide (n = 7). *D*: average ab3A firing rates evoked by linalool oxide (n = 4). Error bars are SEM and are sometimes obscured by markers.

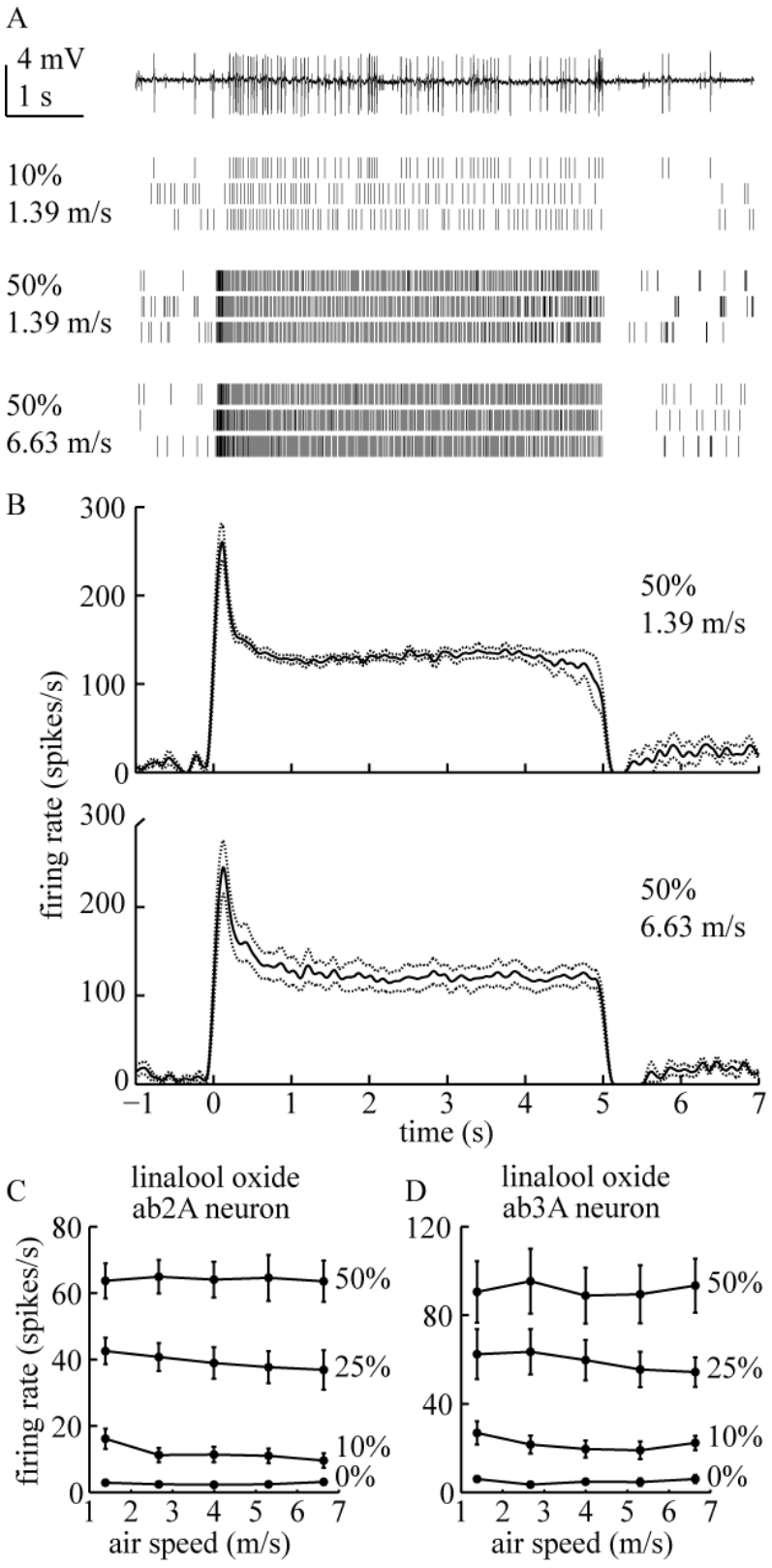

Figure 3.5: (Continued)

In order to test whether there was any statistically significant effect of either stimulus parameter (concentration or air speed) on firing rate, we performed repeated-measures two-way ANOVA tests. For both types of ORNs, we found a highly significant effect of concentration ($p = 5\times10^{-9}$ for ab2A, $p = 5\times10^{-4}$ for ab3A). For ab3A, there was no significant effect of air speed ($p = 0.32$). For ab2A, we did uncover a significant effect of air speed ($p = 0.02$), although the magnitude of this effect is modest. To determine which air speed conditions differed significantly from each other, we performed all possible pair-wise comparisons between air speeds for each concentration in Figure 3.5. None of these comparisons yielded significant differences, except the comparison between the lowest air speed and the highest air speed at the 10% concentration level ($p = 0.02$). However, in this particular set of experiments, we found that the PID voltage showed a significant negative correlation with air speed ($p = 0.01$), indicating that the actual odor concentration delivered to the ORNs was falling as air speed was increasing. Thus, the modest decline in firing rate in this particular set of experiments is likely due to a drop in odor concentration resulting from slight odor leak from the odor delivery device at high pressure, and not a true dependence of ORN firing rate on air speed. Overall, these analyses indicate that there is no significant effect of air speed as long as odor concentration is kept constant.

Next, we repeated these experiments with a highly hydrophobic odor, dibutyl sebacate (water solubility1.6×10^{-4} mol/L). Part of the motivation for this is the fact that moth antennae are reportedly capable of capturing pheromone molecules, and these pheromones are likely to be highly hydrophobic (Kaissling 1971; Kaissling 1986; Kanaujia and Kaissling 1985). Although we could not use insect pheromones in our odor

delivery device, due to our need for large liquid odor volumes and the high cost of pure pheromones, dibutyl sebacate is an 18-carbon long-chain hydrocarbon which has a similar hydrophobicity to pheromones like bombykol. Moreover, of the many long-chain hydrocarbons we tested in pilot experiments, it was the only one that evoked even a moderate excitatory response in the ab3A ORNs. We did not investigate responses to dibutyl sebacate in the ab2A ORNs because it induced inhibition in these neurons, not excitation.

We systematically varied both odor concentration and air speed while recording spikes from ab3A ORNs. We observed that increasing odor concentration increased ORN firing rates, as expected, but increasing air speed did not produce any clear changes (Figure 3.6). Accordingly, a repeated-measures two-way ANOVA showed a highly significant effect of concentration (Figure 3.6, $p = 9\times10^{-8}$), but no significant effect of air speed ($p = 0.11$).

We then repeated these experiments with a highly hydrophilic odor, 1-propanol (water solubility 3.1 mol/L). As before, increasing odor concentration increased firing rates, but there was again no systematic effect of increasing air speed (Figure 3.7). A repeated-measures two-way ANOVA showed a highly significant effect of concentration for both ORN types ($p = 1\times10^{-16}$ for ab2A, $p = 9\times10^{-11}$ for ab3A). For ab3A, there was no significant effect of air speed ($p = 0.08$). For ab2A, we did observe a significant effect of air speed ($p = 3\times10^{-7}$), although the magnitude of this effect is small. Post hoc *t*-tests revealed no significant differences between air speeds for any concentration condition, except a marginal effect for the 40% condition ($p = 0.048$), and in this particular set of experiments the PID values showed a highly significant negative correlation with air

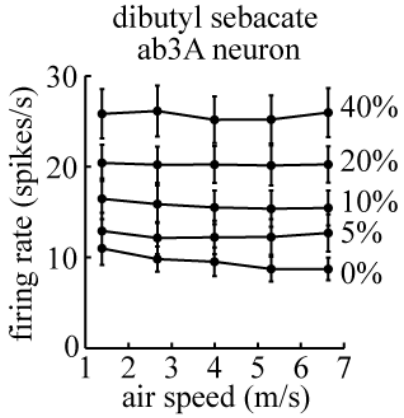

Figure 3.6: ORN responses to dibutyl sebacate depend on concentration but not air speed. Average ab3A firing rates evoked by dibutyl sebacate (n = 6). Responses of ab2A neurons to this odor were inhibitory, and so were not investigated. Error bars are SEM.

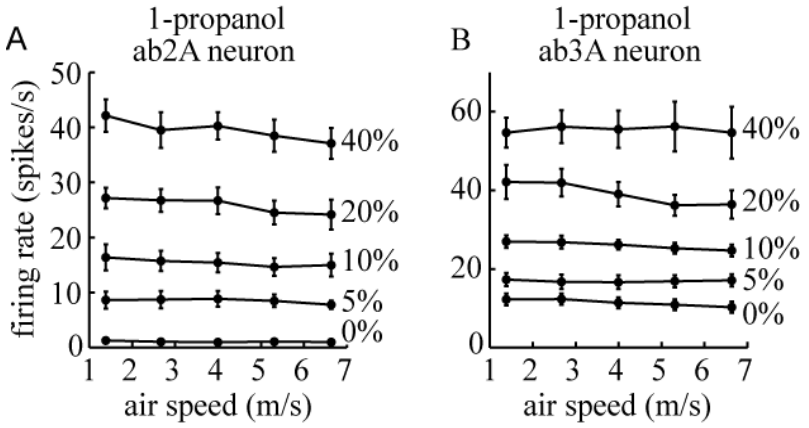

Figure 3.7: ORN responses to 1-propanol depend on concentration but not air speed. *A:* average ab2A firing rates evoked by 1-propanol (n = 9). *C*: average ab3A firing rates evoked by 1-propanol (n = 10). Error bars are SEM and are sometimes obscured by markers.

speed ($p = 2\times10^{-5}$), indicating that the actual odor concentration delivered to the ORNs was dropping as air speed increased. As before, these analyses indicate overall that there is no significant effect of air speed as long as odor concentration is kept constant.

Any boundary layer effects (Figure 3.1B) will be largest in the low air speed regime (Koehl 2006). Therefore, in a final set of experiments, we investigated regimes of even lower air speeds. An additional motivation for these experiments is that the mean flight speed of *Drosophila* is in the range of 0.5-1.0 m/s (Marden et al. 1997), which is near the lower bound of the range that we had used thus far. We therefore explored two additional low-air speed regimes: a range of speeds associated with natural flight (0.22 – 1.35 m/s, Figure 3.8A) and an even lower air speed regime that reaches the limits of our instrumentation (see Methods; 0.06 – 0.22 m/s, Figure 3.8B). (Because each of these two regimes required installing new flow meters in our odor delivery device, they were investigated in separate experiments, and the ORN firing rates we measured in these experiments were not precisely the same as those we measured previously at the same nominal air speeds and concentrations.) As before, we found that varying concentration had a highly significant effect on the firing rate of ab2A for both the intermediate air speed regime (Figure 3.8A, $p = 1\times10^{-11}$) and the lowest regime (Figure 3.8B, $p = 3\times10^{-7}$, repeated-measures two-way ANOVAs). Varying air speed produced no clear changes in firing rate by visual inspection (Figures 3.8A,B), and although ANOVAs examining the effect of air speed did reach the level of statistical significance ($p = 0.02$ for both Figures 3.8A and 3.8B), post hoc *t*-tests did not reveal any significant differences between air speeds. Thus, even in the lowest ranges of air speeds, firing rate does not appear to depend on air speed.

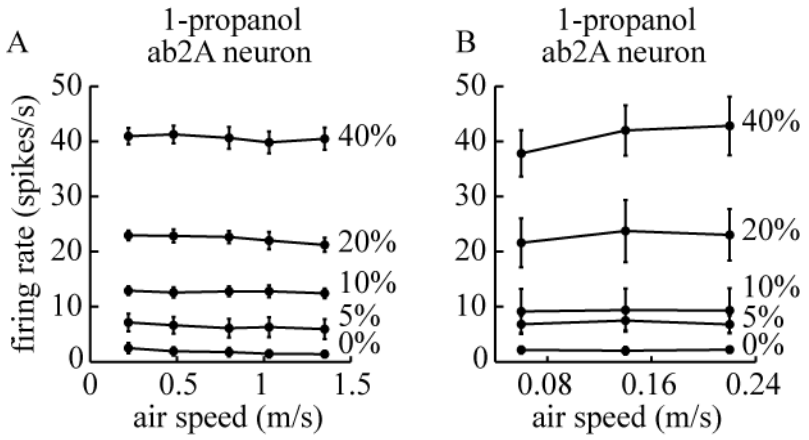

Figure 3.8: ORN responses to 1-propanol are invariant to air speed at a range of low air speeds associated with natural *Drosophila* flight. *A:* average ab2A firing rates evoked by 1-propanol, with air speeds in the range of those experienced by *Drosophila* flying in still air (n = 5). *C*: average ab2A firing rates evoked by 1-propanol, with even lower air speeds than those shown in panel A (n = 7). Error bars are SEM and sometimes obscured by markers.

DISCUSSION

In this study, we were able to achieve an unprecedented level of independent control and validation for two key parameters of olfactory stimuli: odor concentration and air speed. This degree of control allowed us to test rigorously whether transduction in *Drosophila* depends on air speed, as it does on concentration. Our experiments revealed there was no significant effect of air speed on ORN odor responses, as long as odor concentration was held constant while air speed was varied. This finding was consistent across a >100-fold range of air speeds, as well as a >1,000-fold range of odor hydrophobicity values. The same result was observed for two different types of ORNs.

Of course, it is possible that olfactory transduction in other insects might depend on air speed. For example, the moth antenna might differ from the *Drosophila* antenna in this respect, given the difference in the morphology of the antenna in moths versus flies. Whereas the *Drosophila* antenna is a stubby club-like structure, the moth antenna resembles an enormous feather. Also, whereas *Drosophila* sensilla are < 10 microns long, sensilla in some other insects can be 600 microns in length (Keil 1999), and this might magnify boundary-layer effects. We also cannot exclude the idea that *Drosophila* ORNs might show air speed-dependent responses to odors that we did not investigate (e.g., pheromones, which we could not test in our experimental setup). There is evidence that pheromones are delivered to odorant receptors by odorant binding proteins (Xu et al. 2005) and chaperone proteins (Benton et al. 2007), and these co-factors could potentially affect the answer to this question. Nevertheless, our results are likely to generalize to most odors and ORN types in *Drosophila*.

The key finding of this study – that *Drosophila* ORN responses are generally independent of air speed – has implications for the mechanisms of olfactory transduction in this organism. First, it implies that *Drosophila* ORNs are not intrinsically mechanosensitive, at least not in the regime of mechanical forces which we tested. In this respect, *Drosophila* ORNs may differ from vertebrate ORNs (Grosmaitre et al. 2007).

Second, our results do not indicate a role for boundary layer effects, at least on the time scales that we could resolve in this study. The thickness of the boundary layer around the *Drosophila* antenna may simply remain constant over the range of air speeds we have explored. Alternatively, the boundary layer may change thickness, but the rate of diffusion through the layer may not be rate-limiting on the time scales we could resolve. In this study, the time scales where we could potentially resolve any boundary layer effects are limited by the variations in latency from the final valve click to the arrival of odor at the fly. We estimate this latency at ~5 msec at our fastest air speeds and ~500 msec at our slowest air speeds (given a 3-cm distance from the valve to the fly). This means we could not resolve any boundary layer effects that occur on time scales less than ~500 msec. We did not observe any air speed dependence of ORN responses on time scales longer than this (Figure 3.9), and so we do not need to invoke boundary layer effects to explain any of our results.

Third, our results argue that the *Drosophila* antenna does not capture odor molecules with a probability that is invariant to air speed. If the probability of an odor molecule being captured were invariant to air speed, then the rate of odor capture should

Figure 3.9: Dynamics of ORN responses to odor pulses of varying air speeds. Panels show normalized peri-stimulus time histograms of the ab2A neuron's response to a 40% concentration of 1-propanol. *A*: the highest range of air speeds. *B*: an intermediate range of air speeds, including speeds associated with Drosophila flight on a windless day. *C*: the lowest range of air speeds we used in this study. Data in each panel was collected with a different matched pair of flow meters, in separate experiments. These histograms show that, as air speed decreases, the latency of the response increases. Within each panel, latency to reach 50% or 80% peak firing rate was significantly dependent on air speed ($p<0.05$, 1-way repeated measures ANOVA). However, the magnitude of this latency difference can be explained by the increasing delay required for odor to travel from the final valve to the fly. This delay should be ~5 ms for the fastest air speeds we used, and ~500 ms for the slowest air speeds, given the fact that the fly was separated from the final valve by a connector tube 3 cm long. There is also a trend for the rise time of the response to increase with decreasing flow rate, and this likely reflects a tendency for the odor pulse to be smoothed by diffusion. Note that we cannot use the PID to measure the timing of the odor stimulus in all these air speed regimes because the PID does not provide accurate readings below ~2 m/s.

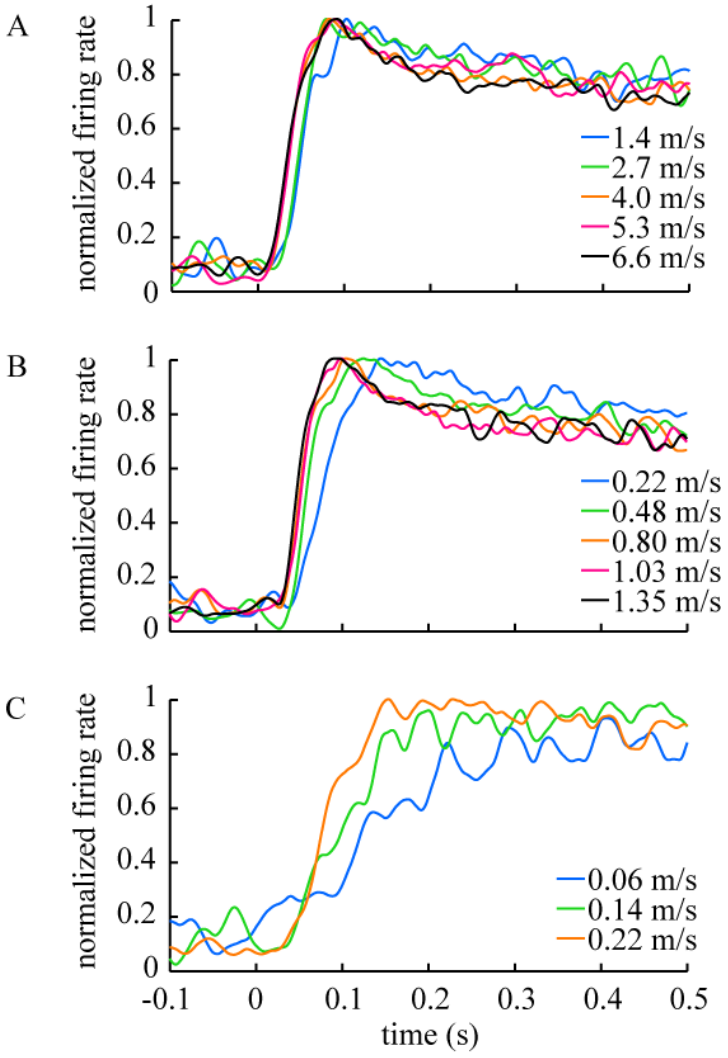

Figure 3.9: (Continued)

be proportional to air speed, and unless some process of odor destruction or removal was also accelerating equally fast, then the local concentration of odor in the antenna should rise with increasing air speed. This would make ORN firing rates grow with increasing air speed, which we do not observe. The idea that the antenna captures odor molecules and does not readily release them has been suggested by the observation that some moth ORN responses far outlast the duration of the nominal stimulus (Kaissling 1971), and this has been cited as evidence for the "sieve" model. Such long-lasting ORN responses can also occur in *Drosophila* ORNs (Montague et al. 2011). However, we find that the incidence of long-lasting responses is dependent on odor concentration but not air speed (Figure 3.10).

Finally, our results imply that pre-absorption phenomena are unlikely to occur in the *Drosophila* antenna. This is hardly surprising, because the *Drosophila* antenna is exposed to ambient air over its entire surface, and so absorption at one end of the antenna should not reduce the concentration delivered to the other end. This stands in contrast to the vertebrate nasal cavity, which forms a long, closed path over which odor can be progressively absorbed.

Invariance to air speed may be adaptive in an organism that has little control over air flow across its antennae. Viewed from this perspective, invariance to air speed can be seen as a feature which should make *Drosophila* olfaction robust to shifting wind conditions. Of course, changes in the wind will also change the structure of turbulent odor plumes (Murlis et al. 1992), and thus olfaction will be indirectly affected. But the intrinsic invariance of this process to air speed may be an advantage to the fly. In contrast to this, it has been suggested that vertebrates actively exploit the dependence of olfactory

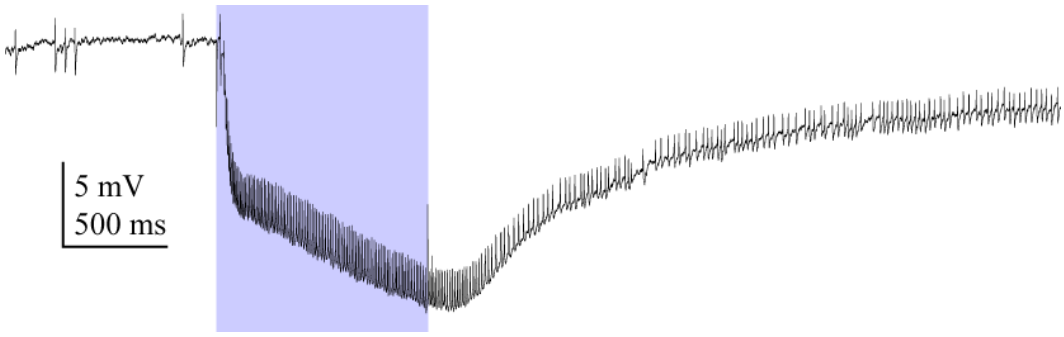

Figure 3.10: An example of a super-sustained ORN response. Sample trace shows an ab3A neuron's response to 100% linalool oxide at an air speed of 2.2 m/s. (This trace was not high-pass filtered, and thus shows both the spiking response of the ab3 neurons and the slower local field potential response.) Odor pulse timing is shown in gray. When these responses did occur, the neuron would often continue to fire at high rates for several minutes. Super-sustained responses like this occurred sporadically under certain stimulus conditions. We found that the probability of observing super-sustained responses increases with odor concentration. Specifically, we observed super-sustained responses in 2 out of 11 recordings where we used 50% linalool oxide, and in 7 out of 9 recordings where we used 100% linalool oxide (all in ab3A neurons). We never observed super-sustained responses in the same neurons when we used lower concentrations of linalool oxide. Although super-sustained responses were correlated with odor concentration, we found no correlation with air speed. In this set of experiments, super-sustained responses occurred at both low air speeds (< 2 m/s, four of 9 cases) and high air speeds (> 2 m/s, five of 9 cases). Thus, super sustained responses appear to be caused by exposure to high odor concentrations, not high air speeds.

transduction on air speed, by manipulating sniff dynamics and thereby manipulating the gradient of odor concentration through the nasal cavity (Schoenfeld and Cleland 2005). These considerations may be relevant not only to the comparative ecology of olfaction, but also to the design of so-called “electronic noses” (Wilson and Baietto 2011), where the regulation of air across the sensor is potentially an important design choice.

REFERENCES

Benton R, Vannice KS, and Vosshall LB. An essential role for a CD36-related receptor in pheromone detection in Drosophila. *Nature* 450: 289-293, 2007.

Couto A, Alenius M, and Dickson BJ. Molecular, anatomical, and functional organization of the Drosophila olfactory system. *Curr Biol* 15: 1535-1547, 2005.

Davis RL. Traces of Drosophila memory. *Neuron* 70: 8-19, 2011.

de Bruyne M, Clyne PJ, and Carlson JR. Odor coding in a model olfactory organ: the Drosophila maxillary palp. *J Neurosci* 19: 4520-4532, 1999.

de Bruyne M, Foster K, and Carlson JR. Odor coding in the Drosophila antenna. *Neuron* 30: 537-552, 2001.

Dethier VG. Sniff, flick, and pulse: an appreciation of interruption. *Proc Am Philos Soc* 131: 159-176, 1987.

Doving KB. Response properties of neurones in the rat olfactory bulb to various parameters of odour stimulation. *Acta Physiol Scand* 130: 285-298, 1987.

Fishilevich E, and Vosshall LB. Genetic and functional subdivision of the Drosophila antennal lobe. *Curr Biol* 15: 1548-1553, 2005.

Grosmaitre X, Santarelli LC, Tan J, Luo M, and Ma M. Dual functions of mammalian olfactory sensory neurons as odor detectors and mechanical sensors. *Nat Neurosci* 10: 348-354, 2007.

Hallem EA, and Carlson JR. The odor coding system of Drosophila. *Trends Genet* 20: 453-459, 2004.

Kaissling K-E. Insect Olfaction. In: *Handbook of Sensory Physiology: Olfaction*, edited by Beidler LM. Heidelberg: Springer Verlag, 1971, p. 351-431.

Kaissling KE. Chemo-electrical transduction in insect olfactory receptors. *Annu Rev Neurosci* 9: 121-145, 1986.

Kaissling KE. Flux detectors versus concentration detectors: two types of chemoreceptors. *Chem Senses* 23: 99-111, 1998.

Kaissling KE. Olfactory perireceptor and receptor events in moths: a kinetic model. *Chem Senses* 26: 125-150, 2001.

Kaissling KE, and Rospars JP. Dose-response relationships in an olfactory flux detector model revisited. *Chem Senses* 29: 529-531, 2004.

Kanaujia S, and Kaissling K-E. Interactions of pheromone with moth antennae: adsorption, desorption and transport. *J Insect Physiol* 31: 71-81, 1985.

Keil TA. Morphology and development of the peripheral olfactory organs. In: *Insect Olfaction*, edited by Hansson BS. Berlin: Springer-Verlag, 1999, p. 6-47.

Kent PF, Mozell MM, Murphy SJ, and Hornung DE. The interaction of imposed and inherent olfactory mucosal activity patterns and their composite representation in a mammalian species using voltage-sensitive dyes. *J Neurosci* 16: 345-353, 1996.

Kepecs A, Uchida N, and Mainen ZF. Rapid and precise control of sniffing during olfactory discrimination in rats. *J Neurophysiol* 98: 205-213, 2007.

Koehl MA. The fluid mechanics of arthropod sniffing in turbulent odor plumes. *Chem Senses* 31: 93-105, 2006.

Laing DG. Natural sniffing gives optimum odour perception for humans. *Perception* 12: 99-117, 1983.

Lansky P, and Rospars JP. Odorant concentration and receptor potential in olfactory sensory neurons. *Biosystems* 48: 131-138, 1998.

Le Magnen J. Étude des facteurs dynamiques de l'excitation olfactive. *Annee Psychol* 45: 77-89, 1944.

Loudon C, and Koehl MA. Sniffing by a silkworm moth: wing fanning enhances air penetration through and pheromone interception by antennae. *J Exp Biol* 203: 2977-2990, 2000.

Mamiya A, Straw AD, Tomasson E, and Dickinson MH. Active and passive antennal movements during visually guided steering in flying Drosophila. *J Neurosci* 31: 6900-6914, 2011.

Marden JH, Wolf MR, and Weber KE. Aerial performance of Drosophila melanogaster from populations selected for upwind flight ability. *J Exp Biol* 200: 2747-2755, 1997.

Masse NY, Turner GC, and Jefferis GS. Olfactory information processing in Drosophila. *Curr Biol* 19: R700-713, 2009.

Montague SA, Mathew D, and Carlson JR. Similar odorants elicit different behavioral and physiological responses, some supersustained. *J Neurosci* 31: 7891-7899, 2011.

Moore PA, Gerhardt GA, and Atema J. High resolution spatio-temporal analysis of aquatic chemical signals using microelectrochemical electrodes. *Chem Senses* 14: 829-840, 1989.

Mozell MM, and Jagodowicz M. Chromatographic separation of odorants by the nose: retention times measured across in vivo olfactory mucosa. *Science* 181: 1247-1249, 1973.

Mozell MM, Kent PF, and Murphy SJ. The effect of flow rate upon the magnitude of the olfactory response differs for different odorants. *Chem Senses* 16: 631-649, 1991a.

Mozell MM, Kent PF, Scherer PW, Hornung DE, and Murphy SJ. Nasal airflow. In: *Smell and Taste in Health and Disease*, edited by Getchell TV, Doty RL, Bartoshuk LM, and Snow JBJ. New York, NY: Raven Press, 1991b.

Murlis J, Elkinton JS, and Cardé RT. Odor plumes and how insects use them. *Annu Rev Entymol* 37: 505-532, 1992.

Olsen SR, and Wilson RI. Cracking neural circuits in a tiny brain: new approaches for understanding the neural circuitry of Drosophila. *Trends Neurosci* 31: 512-520, 2008.

Ramdya P, and Benton R. Evolving olfactory systems on the fly. *Trends Genet* 26: 307-316, 2010.

Rehn T. Perceived odor intensity as a function of air flow through the nose. *Sens Processes* 2: 198-205, 1978.

Rospars JP, Krivan V, and Lansky P. Perireceptor and receptor events in olfaction. Comparison of concentration and flux detectors: a modeling study. *Chem Senses* 25: 293-311, 2000.

Schneider RA, Costiloe JP, Vega A, and Wolf S. Olfactory threshold technique with nitrogen dilution of n-butane and gas chromatography. *J Appl Physiol* 18: 414-417, 1963.

Schoenfeld TA, and Cleland TA. The anatomical logic of smell. *Trends Neurosci* 28: 620-627, 2005.

Scott JW, Acevedo HP, and Sherrill L. Effects of concentration and sniff flow rate on the rat electroolfactogram. *Chem Senses* 31: 581-593, 2006.

Sobel EC, and Tank DW. Timing of odor stimulation does not alter patterning of olfactory bulb unit activity in freely breathing rats. *J Neurophysiol* 69: 1331-1337, 1993.

Wilson AD, and Baietto M. Advances in electronic-nose technologies developed for biomedical applications. *Sensors* 11: 1105-1176, 2011.

Xu P, Atkinson R, Jones DN, and Smith DP. Drosophila OBP LUSH is required for activity of pheromone-sensitive neurons. *Neuron* 45: 193-200, 2005.

Yalkowsky SH, He Y, and Jain P. *Handbook of Aqueous Solubility*. Boca Raton, FL: CRC Press, 2010.

CHAPTER 4:

Conclusion

In this dissertation, I have described two studies investigating chemosensation in *Drosophila*.

In Chapter 2, I described our efforts toward identifying and characterizing central gustatory neurons in *Drosophila*. This study was motivated by how little was known about the central processing of gustatory information in *Drosophila*. Because of this, we had to develop a strategy to establishing functional connectivity within the *Drosophila* gustatory system. Our approach was to use calcium imaging in conjunction with photo-activatable GFP. We were ultimately unsuccessful in our endeavor to identify central gustatory neurons. However, we believe that the problem was not our general approach but rather a lack of specific Gal4 lines. We believe that our strategy in identifying groups of neurons functionally and anatomically connected to peripheral sensory neurons is applicable to generating good candidate central neurons associated with other senses.

Prior to the work in Chapter 3, there had been much speculation but no direct test of whether olfactory transduction in insects depends on air speed. Our results demonstrate that *Drosophila* ORN odor responses are invariant to air speed, as long as odor concentration is kept constant. Our result suggests that olfactory stimuli in *Drosophila* are not transduced through force gated ion channels. It also argues against several classes of models of odor absorption and delivery. Finally, our finding suggests that the evolution of air speed-invariant olfactory transduction in *Drosophila* may be an adaptation to their inability to control air speed at their olfactory organ. This stands in contrast to terrestrial vertebrates, which can control air speed through the nose, and which

are thought to actively exploit the air speed-dependence of olfactory transduction to modulate it.

Moving forward, as we learn more about gustatory processing, it will be interesting to compare and contrast it with olfactory processing. Although the two share some homology at the level of their peripheral receptors, it is unclear as to how closely the two resemble each other as we move more centrally.